Decentralized Robust Control for Vehicle Platooning Subject to Uncertain Disturbances via Super-Twisting Second-Order Sliding-Mode Observer Technique

Jianshan Zhou, Daxin Tian, *Senior Member, IEEE*, Zhengguo Sheng, *Senior Member, IEEE*, Xuting Duan, Guixian Qu, Dongpu Cao, *Member, IEEE*, and Xuemin Shen, *Fellow, IEEE*

***Abstract*—Platoon-based vehicular cyber-physical systems (VCPSs) have attracted much attention due to their potential to improve road capacity and energy efficiency. However, the comprehensive effect of the mismatched modeling dynamics and unknown disturbances can impose a great challenge on the convergence and stability of vehicle platooning. In this paper, we propose a novel decentralized robust control approach to address the external disturbances in vehicle platooning. Specifically, by combining a super-twisting second-order sliding mode (SOSM) strategy and a disturbance observer (DO), we design a super-twisting SOSMDO platoon controller. We also derive some design conditions of the controller and observer gains. Using the Lyapunov methodology, we theoretically prove under the design conditions the finite-time convergence of the super-twisting SOSMDO to the platooning equilibrium state and its closed-loop stability to the disturbances. Extensive simulations have been conducted and the results demonstrate the superior performance of the proposed control approach in terms of inter-vehicle spacing, velocity tracking, and platoon robustness.**

***Index Terms*—Disturbance observer, sliding mode control, stability, vehicle platoon.**

Manuscript received August 17, 2021; revised December 3, 2021; accepted April 22, 2022. Date of publication April 27, 2022; date of current version July 18, 2022. This work was supported in part by the National Postdoctoral Program for Innovative Talents under Grant BX2021027, in part by the China Postdoctoral Science Foundation under Grant 2020M680299, in part by the Opening Project of Ministry of Transport Key Laboratory of Technology on Intelligent Transportation Systems under Grant F20211746, in part by the National Natural Science Foundation of China under Grant U20A20155, and in part by the Beijing Municipal Natural Science Foundation under Grant L191001. The review of this article was coordinated by Prof. James Anderson. *(Corresponding author: Daxin Tian.)*

Jianshan Zhou, Daxin Tian, and Xuting Duan are with the Beijing Advanced Innovation Center for Big Data and Brain Computing, Beijing Key Laboratory for Cooperative Vehicle Infrastructure Systems & Safety Control, School of Transportation Science and Engineering, Beihang University, Beijing 100191, China (e-mail: jianshanzhou@foxmail.com; dtian@buaa.edu.cn; duanxuting@buaa.edu.cn).

Guixian Qu is with the Aero-engine System Collaborative Design Center, Research Institute of Aero-Engine, Beihang University, Beijing 100191, China (e-mail: guixianqu@foxmail.com).

Zhengguo Sheng is with the Department of Engineering and Design, University of Sussex, Richmond 3A09, U.K. (e-mail: z.sheng@sussex.ac.uk).

Dongpu Cao is with the Department of Mechanical and Mechatronics Engineering, University of Waterloo, Waterloo, ON N2L3G1, Canada (e-mail: dongpu.cao@uwaterloo.ca).

Xuemin Shen is with the Electricaland Computer Engineering Department, University of Waterloo, Waterloo, ON N2L 3G1, Canada (e-mail: sshen@uwaterloo.ca).

Digital Object Identifier 10.1109/TVT.2022.3170572

I. Introduction

CONNECTED and automated vehicles (CAVs) have been considered as a promising system component for revolutionizing social mobility. In particular, automated vehicles moving as platoons, i.e., platooning vehicles in a closely spacing group, are expected to dramatically improve driving experience, traffic efficiency and safety, road capacity, and also reduce energy consumption in road transportation systems [1]–[3]. With recent advances in wireless communications and edge computing, intelligent vehicles can be equipped with vehicle-to-vehicle (V2V) and vehicle-to-infrastructure (V2I) communications to exchange real-time information, process data-massive and latency-critical applications, and thus enable the autonomous coordination among themselves [4], [5]. Therefore, over the past several decades, the interaction, automation, and coordination of platooning vehicles have attracted increasing attention from both academia and industry. In order to ensure safe and reliable mobility, automatic control of closely spaced platoons is required. More importantly, control stability and robustness are critical and should be guaranteed for vehicle platooning in a real complex environment.

A. Literature Review

Many vehicle platooning or interconnected system control strategies have been proposed in the current literature [1], [2], among which the constant spacing (CS) policy [6] and the constant time headway (CTH) policy [7], [8] are most commonly exploited since they can be practically implemented with low complexity. Based on the CS or the CTH policies, extensive advanced adaptive cruise control (ACC) and cooperative adaptive cruise control (CACC) schemes have been currently developed by combining different adaptive mechanisms, such as the parameter-space linear quadratic regulator-based CACC approach [9], the communication delay-compensated approach [10], the acceleration/control feedback-based approach [11], the infrastructure-assisted linear ACC [12], and many others [13]–[17]. Although a broad range of traditional ACC and CACC controllers based on the CS or CTH policies can bring a promising performance and simplify system deployment, they have some restrictions in reality. Namely, their implementation requires full or partial accurate state information. The linear time-invariant controller

gains are usually designed without compensating the effect of external unknown disturbances.

To cope with the external disturbances or uncertain system dynamics, other control designs are proposed based on the well-known linear matrix inequality (LMI) method and robust H-infinity control theory [18]–[23]. The robust H-infinity control approaches aim to achieve the platoon string stability by guaranteeing the worst-case control performance that is usually measured by the H-infinity norm. In essence, these approaches also rely on the state feedback/feedforward to realize robust controllers. However, their static state feedback/feedforward gains do not take into account the dynamic disturbance compensation and require solving a worst-case optimization problem that involves complicated nonlinear constraints in the vehicle platooning scenario.

In addition, a wide range of vehicle platoon control approaches are fundamentally based on mathematical optimization theory like [24]–[27], i.e., falling into the specific category of optimal control. In the optimal control paradigm, a control solution is obtained by solving a finite-horizon optimal control problem that usually has an explicit optimization objective and a set of constraints on both the system state and control. According to the control implementation and the time horizon for solving the optimization model, the optimal control can also be divided into two categories, i.e., the rolling horizon control [24], [25] and the model predictive control (MPC) [26], [27]. Nevertheless, the computational efficiency of a constrained optimization model, particularly a nonlinear constrained optimization, remains to be a significant challenge in the online MPC implementation due to the complexity in the optimal control formulation of a vehicle platoon. Even though some remarkable advances have been recently achieved in robust MPC theory such as the representative works based on the invariant tube construction or the worst-case optimization [28]–[30], these robust MPC approaches have to face the increased computational complexity resulting from either solving dramatically high-dimensional LMIs or addressing a sequence of robust positively invariant (RPI) sets.

Besides, to robustly deal with the mismatched nonlinearity and uncertain disturbances, many other studies resort to the sliding mode control theory [31]–[34]. For example, in [31], a decentralized sliding-mode control approach has been proposed by combining a nonlinear disturbance observer with the first-order sliding mode control. The design conditions on the controller and the observer gains for guaranteeing the robust stability are obtained by matrix transformation and decomposition, which inevitably involves the complex computation. In [32], the sliding mode control is applied to realize the distributed control of vehicles approaching a traffic signal intersection. But it does not explicitly account for the external unknown disturbances in the vehicle dynamics. In [33], a distributed sliding mode control model has been developed based on a topologically structured function. The authors define the combined tracking error incorporated in the sliding mode dynamics in terms of the longitudinal position and velocity deviations from their desired counterparts [33]. Similarly, [34] also defines a distributed sliding mode surface by combining both the position and velocity tracking errors and adopts an exponential reaching law to design a distributed adaptive sliding mode controller for a vehicle platoon subject to the external unknown disturbances. Some linear matrix inequality conditions need to be solved to determine an appropriate pole placement of the sliding motion dynamics [34]. From the above works, it is witnessed that classic sliding mode control approaches can provide high-accuracy tracking performance and favorable robustness to the external disturbances for a disturbed vehicle platoon. However, the aforementioned control approaches based on classic sliding modes are limited in two aspects: on one side, their control variables need to appear in the first-order time derivative of the tracking error, which cannot incorporate the lower-layer dynamics (e.g., the acceleration variation) of the vehicles; on the other side, the first-order sliding modes has only one relative degree, and although the sliding mode variable is continuous, its time derivative may be discontinuous. As a consequence, the classic sliding mode control approaches may heavily experience the so-called chattering effect, i.e., the high-frequency control switching.

The sliding mode control methodology can also be integrated with some other mechanisms, such as the upper-layer trajectory optimization [35], the prescribed tracking strategy [36], the nonzero-initial spacing error transformation [37], and the bidirectional information interaction strategy [38], to enhance its platoon control performance. In [39], the authors propose a distributed integral sliding mode controller for cooperative braking of vehicles in a platoon. However, in these works [35]–[39], the lower-layer tracking error dynamics, such as the time derivative of the longitudinal acceleration, has not been taken into consideration in the design of their sliding mode surfaces. Besides, the perturbation reconstruction has not been explored in their sliding-mode control loop. In some other works like [40], [41], the integration of a nonlinear disturbance observer from [42]–[44] and an integral sliding mode controller is shown to be powerful to achieve the control robustness. The integral sliding mode controller with a observer can use the perturbation reconstruction to compensate the external disturbances. However, in these works [40], [41], the conventional double-integrator vehicle model (i.e., a second-order kinematic model) is adopted such that it cannot incorporate the lower-layer vehicle dynamics into the control design. Additionally, their observer's gains need to be carefully selected, while the explicit design conditions for their observer's gains remain to be theoretically unexplored.

B. Motivation and Contribution

Even though a wide variety of state feedback/feedforward-based linear control designs have been developed and analyzed in the current literature, the finite-time convergence of the vehicles' tracking errors, low-complexity gain design conditions, and theoretically-guaranteed strong robustness remain to be explored in vehicle platooning subject to the external unknown disturbances. In particular, even though traditional first-order sliding mode control approaches can provide robust and high-accuracy control solutions under the external disturbances, they may face the chattering effect in high-frequency control switching. To bridge the gap, we are motivated by the higher-order sliding modes [45]–[49].

Specifically, in this paper, we propose a decentralized robust platoon control approach based on the super-twisting second-order sliding mode (SOSM). Nonetheless, we do not apply the existing super-twisting SOSM for vehicle platooning directly, which essentially differentiates our work to the existing literature [35]–[41]. Instead, we propose a super-twisting SOSM-based disturbance observer (SOSMDO) to reconstruct the uncertain system perturbation term and use the estimated term in the feedback control loop to compensate the effect of the external uncertainties in real-time. This idea yields a novel platoon controller using the super-twisting SOSMDO, which can robustly and asymptotically stabilize the platooning equilibrium in the presence of external unknown disturbances. Additionally, the proposed control approach only needs to appropriately configure a few gain parameters. The sufficient stability conditions of low computational complexity have also been theoretically derived by using the Lyapunov approach. More importantly, the proposed control approach extends, for the first time, the classic sliding mode surface design of only one relative degree in the platoon control context like [31]–[34] to a higher-order formulation for robust vehicle platooning and theoretically guarantees the finite-time convergence of the compensated sliding-mode dynamics subject to any unknown but bounded disturbances. The contributions of our paper are summarized as follows.

i) For the scenario of longitudinal vehicle platooning in the presence of external uncertain but bounded disturbances, we first propose a decentralized super-twisting SOSM platoon controller to maneuver a platoon of vehicles in order to track a reference velocity profile while maintaining a desired inter-vehicle spacing. By using the Lyapunov approach, we also prove the finite-convergence of the designed controller and its robustness to the external disturbances, and derive the sufficient stability conditions for the controller's gains.

ii) To address the issue about the practical implementation of the platoon control in requiring information on the perturbation term, we further propose a nonlinear disturbance observer by leveraging the formulation of the super-twisting SOSM, termed a super-twisting SOSMDO. Using the proposed observer, we are able to reconstruct the disturbance and use its estimation in the feedback loop to compensate the disturbance effect so as to improve the closed-loop adaptability.

iii) With the super-twisting SOSMDO, we design another decentralized platoon controller that is driven by the compensated sliding mode dynamics. It is proved that the new controller can robustly guarantee the asymptotic convergence of the vehicle platoon subject to the external disturbances. Some sufficient stability conditions are also derived for both the controller's and the observer's gains.

The remainder of this paper is organized as follows. In Section II, the vehicle model with the lower-layer dynamics in the presence of external disturbances is introduced and the decentralized platoon control problem is formulated. Next, we propose a decentralized robust controller based on the super-twisting SOSM for vehicle platooning in Section III. A nonlinear disturbance observer in the super-twisting SOSM format is proposed and the super-twisting SOSMDO-based platoon controller is designed as well in Section IV. Section V presents the simulation results that validate the performance of the proposed robust control approach for vehicle platooning. Section VI concludes this work and states the future work.

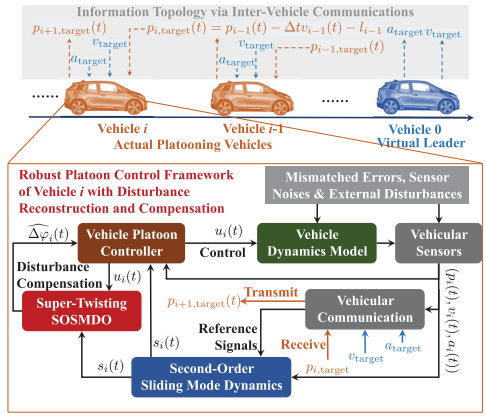

Fig. 1. The application scenario of longitudinal vehicle platooning and our robust platoon control framework.

II. Problem Formulation

Consider a longitudinal platoon of automatically controlled vehicles that can exchange their real-time state and control information via vehicle-to-vehicle (V2V) communications. The number of platooning vehicles is denoted by $(N+1)$, i.e., including one virtual leader and N actual followers as shown in Fig. 1. As shown in Fig. 1, our platoon control is considered to be implemented in a decentralized manner by following a preceding-follower information topology. Let $\mathcal{I}_N := \{1, 2, \ldots, N\}$ denote the set of the following vehicles and $\mathcal{I}_{N+1} := \{0, 1, \ldots, N\}$ the set of the entire platooning vehicles. For each vehicle $i \in \mathcal{I}_{N+1}$, its longitudinal position, velocity, acceleration, and control input at time $t \in \mathbb{R}_{\geq 0}$ are denoted by $p_i(t)$, $v_i(t)$, $a_i(t)$, and $u_i(t)$, respectively. As suggested by current studies [12], [15], [26], [50], the vehicle dynamics can be characterized by combining both the upper-level and the lower-level kinematics and dynamics parameters, which is approximately modeled by

$$\begin{cases} \dot{p}_i(t) = v_i(t), \\ \dot{v}_i(t) = a_i(t), \\ \dot{a}_i(t) = -\frac{1}{\tau} a_i(t) + \frac{\kappa}{\tau} u_i(t), \forall i \in \mathcal{I}_N, \end{cases} \tag{1}$$

where τ denotes the actuation time lag for the vehicle to achieve the requested acceleration, while κ is the ratio of the requested acceleration that can be realized by the vehicle. The three-order approximation model (1) allows for incorporating the nonlinear effects of aerodynamic drag, engine and transmission dynamics, road condition, and some others [18], [51]. Thus, it has been widely adopted as a vehicle model for the controller design in current literature. However, due to the fact that there inherently exist some certain modeling errors (i.e., the mismatched model uncertainties), parametric measurement noises (i.e., sensor information uncertainties), and external uncertain disturbances, the model (1) may fail in capturing the actual dynamics of the vehicle in reality. Therefore, we introduce a lumped uncertainty

term as $\boldsymbol{\omega}_i(t)$, which is a column vector and represents the coupled effect of the aforementioned modeling errors and external disturbances on the longitudinal position, velocity, and acceleration dynamics, respectively. The lumped disturbance term can also represent the mismatched model uncertainties resulting from potential communication delays, data packet losses, and some other unknown system response lags [31]. Then, we extend (1) to a more general model allowing for the external disturbances as the following state-space form

$$\dot{\boldsymbol{x}}_i(t) = \boldsymbol{A}\boldsymbol{x}_i(t) + \boldsymbol{B}u_i(t) + \boldsymbol{C}\boldsymbol{\omega}_i(t), \forall i \in \mathcal{I}_N, \tag{2}$$

where $\boldsymbol{x}_i(t) := [p_i(t), v_i(t), a_i(t)]^{\mathrm{T}}$ is the state variable, $\boldsymbol{C}$ is a known real matrix with compatible dimension, and

$$\boldsymbol{A} := \begin{bmatrix} 0 & 1 & 0 \\ 0 & 0 & 1 \\ 0 & 0 & -\frac{1}{\tau} \end{bmatrix}, \boldsymbol{B} := \begin{bmatrix} 0 \\ 0 \\ \frac{\kappa}{\tau} \end{bmatrix}. \tag{3}$$

It is noted that the whole term $\boldsymbol{C}\boldsymbol{\omega}_i(t)$ represents the effect of the external disturbances. The coefficient matrix $\boldsymbol{C}$ is used to denote the scaling factor and linear transformation on the elements of $\boldsymbol{\omega}_i(t)$, which is of $3 \times n_{\boldsymbol{\omega}_i(t)}$ size where $n_{\boldsymbol{\omega}_i(t)}$ is the row number of the disturbance vector $\boldsymbol{\omega}_i(t)$. In practice, the lumped disturbance term $\boldsymbol{\omega}_i(t), i \in \mathcal{I}_N$, as well as its firs-order time derivative, $\dot{\boldsymbol{\omega}}_i(t)$, is usually bounded as

$$\begin{cases} \sup\limits_{t\in\mathbb{R}_{\geq 0}} \|\boldsymbol{\omega}_i(t)\|_\infty \leq \eta_i, \\ \sup\limits_{t\in\mathbb{R}_{\geq 0}} \|\dot{\boldsymbol{\omega}}_i(t)\|_\infty \leq \Delta\eta_i, \end{cases} \tag{4}$$

where η_i and $\Delta\eta_i$ are some upper bounds known for $i \in \mathcal{I}_N$.

Given (2), the problem of cooperative platooning of the connected and automated vehicles can be realized by a constant time-headway spacing policy that is formulated as a second-order consensus problem. To be specific, the platooning vehicles need to maintain a desired inter-vehicle time headway Δt and track a desired velocity v_{target} of the platoon. Mathematically, the objective of our control design is to drive the longitudinal positions and velocities of all the platooning vehicles toward the desired steady state as follows

$$\begin{cases} \lim\limits_{t\to\infty} |p_{i-1}(t) - \Delta t v_i(t) - l_{i-1} - p_i(t)| = 0, \\ \lim\limits_{t\to\infty} |v_{i-1}(t) - v_i(t)| = 0, \end{cases} \tag{5}$$

for all $i \in \mathcal{I}_N$, where l_i denotes the length of the vehicle i. It is remarked that the trajectory profile $(p_0(t), v_0(t))$ of the virtual leading vehicle is assumed to be known and treated as the reference signal for its followers. Moreover, another goal of our work is to guarantee the stability, especially the finite-time convergence and robustness, of the platoon under the designed control subject to external uncertain disturbances.

III. Decentralized Robust Controller Design

To design a decentralized controller for each platooning vehicle $i \in \mathcal{I}_N$, the real-time longitudinal position and velocity profiles of a platooning vehicle $i-1$ can be treated as a reference signal for its immediate follower i. Such a reference signal is considered to be fed backward from $i-1$ to i via V2V communications as shown in Fig. 1. For the sake of convenience, we denote the reference position profile for each follower $i \in \mathcal{I}_N$ by $p_{i,\text{target}}(t) := p_{i-1}(t) - \Delta t v_{i-1}(t) - l_{i-1}$. To realize tracking of the desired position and velocity, we define the linearly weighted combination of both the position and velocity tracking errors, $e_{1,i}(t)$, and its first-order derivative, $e_{2,i}(t)$, for any $i \in \mathcal{I}_N$, as follows

$$\begin{cases} e_{1,i}(t) = p_{i,\text{target}}(t) - p_i(t) + b_{1,i}\left(v_{\text{target}} - v_i(t)\right) \\ e_{2,i}(t) = v_{\text{target}} - v_i(t) + b_{2,i}\left(a_{\text{target}} - a_i(t)\right) \end{cases} \tag{6}$$

where $b_{1,i}$ and $b_{2,i}$ denote the positive coefficients weighing the influence of the velocity tracking error and that of its derivative on the entire sliding surface, respectively. In (6), since the constant time headway spacing policy is adopted, the reference acceleration a_{target} at the equilibrium state is indeed set to $a_{\text{target}} = \dot{v}_{\text{target}} = 0$.

According to the control objective represented by (5), we exploit the super-twisting SOSM theory and introduce a sliding mode surface, denoted by a variable $s_i(t)$, for each $i \in \mathcal{I}_N$. Specifically, $s_i(t)$ can be designed as follows [45]–[47]

$$s_i(t) = c_i e_{1,i}(t) + e_{2,i}(t), i \in \mathcal{I}_N, \tag{7}$$

where c_i is a positive coefficient weighing the influence of the first-order tracking error on the sliding mode surface. It is remarked here that the design of our sliding mode surface based on (6) and (7) is quite different from the existing studies [31]–[41] in the field of the sliding mode control-based vehicle platooning. Our sliding mode surface in (6) and (7) incorporates the high-order characteristics and allows for the lower-layer vehicle dynamics in (1), i.e., the time-varying longitudinal acceleration.

To proceed, we combine (2) and (7) to further obtain

$$\dot{s}_i(t) = \varphi\left(t, \boldsymbol{x}_i(t), \boldsymbol{\omega}_i(t)\right) - K_i u_i(t), i \in \mathcal{I}_N, \tag{8}$$

where $\varphi(t, \boldsymbol{x}_i(t), \boldsymbol{\omega}_i(t))$ is given as

$$\varphi\left(t, \boldsymbol{x}_i(t), \boldsymbol{\omega}_i(t)\right) = \boldsymbol{k}_{i,1}\boldsymbol{x}_i(t) + \boldsymbol{k}_{i,2}\boldsymbol{\omega}_i(t) + c_i\dot{p}_{i,\text{target}}(t) \tag{9}$$

and

$$K_i = \frac{b_{2,i}\kappa}{\tau}. \tag{10}$$

In (9), $\boldsymbol{k}_{i,1}$, $\boldsymbol{k}_{i,2}$, $i \in \mathcal{I}_N$, are row vectors given as follows

$$\begin{aligned} \boldsymbol{k}_{i,1} &= -\left[0 \quad c_i \quad \left(c_i b_{1,i} + 1 - \tfrac{b_{2,i}}{\tau}\right)\right], \\ \boldsymbol{k}_{i,2} &= -\left[c_i\boldsymbol{C}_1 + \left(c_i b_{1,i} + 1\right)\boldsymbol{C}_2 + b_{2,i}\boldsymbol{C}_3\right], \end{aligned} \tag{11}$$

where $\boldsymbol{C}_l$ denotes the l-th row vector of $\boldsymbol{C}$, $l = 1, 2, 3$.

Remark that the state $\boldsymbol{x}_i(t)$ is bounded in an actual application scenario, and the lumped external disturbance $\boldsymbol{\omega}_i(t)$ and its time derivative $\dot{\boldsymbol{\omega}}_i(t)$ are also bounded. Due to the boundedness in the system state and the disturbance dynamics, there exist some positive constants $\theta_i^* > 0$ such that $\varphi(t, \boldsymbol{x}_i(t), \boldsymbol{\omega}_i(t))$ in (9) can be bounded as [45], [46], [49]

$$\left|\varphi\left(t, \boldsymbol{x}_i(t), \boldsymbol{\omega}_i(t)\right)\right| \leq \theta_i^* \left|s_i(t)\right|^{\frac{1}{2}}, i \in \mathcal{I}_N. \tag{12}$$

Therefore, there also exist some certain positive $\theta_i \in (0, \theta_i^*]$ such that $\varphi(t, \boldsymbol{x}_i(t), \boldsymbol{\omega}_i(t))$ satisfies, according to the intermediate

value theorem,

$$\varphi\left(t, \boldsymbol{x}_i(t), \boldsymbol{\omega}_i(t)\right) = \theta_i \left|s_i(t)\right|^{\frac{1}{2}} \operatorname{sign}\left(s_i(t)\right), i \in \mathcal{I}_N. \quad (13)$$

Recalling (5), the platoon control boils down to stabilizing the dynamics of the sliding mode surface in (8), and more importantly, guaranteeing that the sliding mode variable $s_i(t)$ in (7) can converge to the origin in finite time. To achieve this goal, we design a control law based on the super-twisting SOSM theory as follows [48], [49]

$$u_i(t) = \alpha_i \left|s_i(t)\right|^{\frac{1}{2}} \operatorname{sign}\left(s_i(t)\right) + \beta_i \int_0^t \operatorname{sign}\left(s_i(\sigma)\right) d\sigma \quad (14)$$

for each $i \in \mathcal{I}_N$, and choose the control gains α_i and β_i by following the constraints

$$\begin{cases} \alpha_i > \frac{\theta_i}{K_i}, \\ \beta_i > \frac{K_i \alpha_i^2 (\theta_i - K_i \alpha_i)}{4(K_i \alpha_i - 2\theta_i)}. \end{cases} \quad (15)$$

For the designs in (14) and (15), we have the following result.

Theorem 1: For any $i \in \mathcal{I}_N$, suppose that the disturbance term $\varphi(t, \boldsymbol{x}_i(t), \boldsymbol{\omega}_i(t))$ is bounded as (12). Given that the control law $u_i(t)$ follows (14) with the gains α_i and β_i satisfying (15), the sliding mode variable $s_i(t)$ in (7) following the dynamics in (8) can converge to the origin in finite time.

Proof: We let $s_{1,i}(t) := s_i(t)$, $K_{\alpha,i} := K_i \alpha_i$, and $K_{\beta,i} := K_i \beta_i$ for the sake of notation simplicity. Additionally, we also introduce an auxiliary variable $s_{2,i}(t)$ that captures the switching dynamics of the sign of $s_i(t)$, i.e., $s_{2,i}(t) = -\int_0^t K_{\beta,i} \operatorname{sign}(s_{1,i}(\sigma)) d\sigma$. Substituting the control law (14) into (8) can yield

$$\begin{cases} \dot{s}_{1,i}(t) = -K_{\alpha,i} \left|s_{1,i}(t)\right|^{\frac{1}{2}} \operatorname{sign}\left(s_{1,i}(t)\right) + s_{2,i}(t) \\ \qquad\qquad + \varphi\left(t, \boldsymbol{x}_i(t), \boldsymbol{\omega}_i(t)\right), \\ \dot{s}_{2,i}(t) = -K_{\beta,i} \operatorname{sign}\left(s_{1,i}(t)\right). \end{cases} \quad (16)$$

Using the transformation approach presented in [45]–[49], we introduce an auxiliary state variable as

$$\boldsymbol{\xi}_i(t) = \begin{bmatrix} \left|s_{1,i}(t)\right|^{\frac{1}{2}} \operatorname{sign}\left(s_{1,i}(t)\right), \\ -K_{\beta,i} \int_0^t \operatorname{sign}\left(s_{1,i}(\sigma)\right) d\sigma \end{bmatrix}, i \in \mathcal{I}_N. \quad (17)$$

Based on (17), a candidate Lyapunov function for analyzing the system convergence and stability can be formulated as

$$\begin{aligned} V_i\left(\boldsymbol{\xi}_i(t)\right) &= 2K_{\beta,i} \left|s_{1,i}(t)\right| + \frac{1}{2} s_{2,i}^2(t) \\ &\quad + \frac{1}{2} \left(K_{\alpha,i} \left|s_{1,i}(t)\right|^{\frac{1}{2}} \operatorname{sign}\left(s_{1,i}(t)\right) - s_{2,i}(t)\right)^2 \\ &= \boldsymbol{\xi}_i^{\mathrm{T}}(t) \boldsymbol{P}\left(K_{\alpha,i}, K_{\beta,i}\right) \boldsymbol{\xi}_i(t), i \in \mathcal{I}_N, \end{aligned} \quad (18)$$

where the matrix $\boldsymbol{P}(K_{\alpha,i}, K_{\beta,i})$ depends on the gains $K_{\alpha,i}$ and $K_{\beta,i}$ as follows

$$\boldsymbol{P}\left(K_{\alpha,i}, K_{\beta,i}\right) = \frac{1}{2} \begin{bmatrix} 4K_{\beta,i} + K_{\alpha,i}^2 & -K_{\alpha,i} \\ -K_{\alpha,i} & 2 \end{bmatrix}. \quad (19)$$

Besides, for any $i \in \mathcal{I}_N$, the time derivative of the new state variable $\boldsymbol{\xi}_i(t)$ is

$$\dot{\boldsymbol{\xi}}_i(t) = \frac{1}{\left|\xi_{1,i}(t)\right|} \begin{bmatrix} \frac{-K_{\alpha,i}\xi_{1,i}(t) + \xi_{2,i}(t) + \varphi(t, \boldsymbol{x}_i(t), \boldsymbol{\omega}_i(t))}{2} \\ -K_{\beta,i}\xi_{1,i}(t) \end{bmatrix}, \quad (20)$$

where $\xi_{1,i}(t)$ and $\xi_{2,i}(t)$ are the first and the second elements of the column state vector $\boldsymbol{\xi}_i(t)$, respectively, and $|\xi_{1,i}(t)|$ is $|\xi_{1,i}(t)| = |s_{1,i}(t)|^{\frac{1}{2}}$. Using (20), the dynamics in (16) can be rearranged as the compact form

$$\dot{\boldsymbol{\xi}}_i(t) = \frac{1}{\left|\xi_{1,i}(t)\right|} \left[\boldsymbol{Q}\left(K_{\alpha,i}, K_{\beta,i}\right) \boldsymbol{\xi}_i(t) + \boldsymbol{\varphi}_i\right], \quad (21)$$

where we define

$$\begin{aligned} \boldsymbol{Q}\left(K_{\alpha,i}, K_{\beta,i}\right) &= \frac{1}{2} \begin{bmatrix} -K_{\alpha,i} & 1 \\ -2K_{\beta,i} & 0 \end{bmatrix}, \\ \boldsymbol{\varphi}_i &= \frac{1}{2} \begin{bmatrix} \varphi\left(t, \boldsymbol{x}_i(t), \boldsymbol{\omega}_i(t)\right) \\ 0 \end{bmatrix}. \end{aligned} \quad (22)$$

Recalling $\varphi(t, \boldsymbol{x}_i(t), \boldsymbol{\omega}_i(t)) = \theta_i \xi_{1,i}(t)$ in (13), $\boldsymbol{\varphi}_i$ can be decomposed as $\boldsymbol{\varphi}_i = \boldsymbol{\Lambda}_i \boldsymbol{\xi}_i(t)$, where $\boldsymbol{\Lambda}_i$ is given by

$$\boldsymbol{\Lambda}_i = \frac{1}{2} \begin{bmatrix} \theta_i & 0 \\ 0 & 0 \end{bmatrix}. \quad (23)$$

Hence, based on (18) and (21), we obtain the time derivative of the Lyapunov function $V_i(t)(\boldsymbol{\xi}_i(t))$ as follows

$$\begin{aligned} \dot{V}_i\left(\boldsymbol{\xi}_i(t)\right) &= \frac{1}{\left|\xi_{1,i}(t)\right|} \boldsymbol{\xi}_i^{\mathrm{T}}(t) \left(\boldsymbol{Q}_i^{\mathrm{T}} \boldsymbol{P}_i + \boldsymbol{P}_i \boldsymbol{Q}_i\right) \boldsymbol{\xi}_i(t) \\ &\quad + \frac{2}{\left|\xi_{1,i}(t)\right|} \boldsymbol{\xi}_i^{\mathrm{T}}(t) \boldsymbol{P}_i \boldsymbol{\Lambda}_i \boldsymbol{\xi}_i(t) \\ &= -\frac{1}{\left|\xi_{1,i}(t)\right|} \boldsymbol{\xi}_i^{\mathrm{T}}(t) \boldsymbol{\Phi}_i \boldsymbol{\xi}_i(t), i \in \mathcal{I}_N, , \end{aligned} \quad (24)$$

where $\boldsymbol{Q}_i := \boldsymbol{Q}(K_{\alpha,i}, K_{\beta,i})$ and $\boldsymbol{P}_i := \boldsymbol{P}(K_{\alpha,i}, K_{\beta,i})$ for the sake of simplicity. The matrix $\boldsymbol{\Phi}_i$ is given as follows

$$\begin{aligned} \boldsymbol{\Phi}_i &= -\left(\boldsymbol{Q}_i^{\mathrm{T}} \boldsymbol{P}_i + \boldsymbol{P}_i \boldsymbol{Q}_i\right) - 2\boldsymbol{P}_i \boldsymbol{\Lambda}_i \\ &= \frac{K_{\alpha,i}}{2} \begin{bmatrix} K_{\alpha,i}^2 + 2K_{\beta,i} - \theta_i \left(K_{\alpha,i} + \frac{4K_{\beta,i}}{K_{\alpha,i}}\right) & -K_{\alpha,i} \\ -\left(K_{\alpha,i} - \theta_i\right) & 1 \end{bmatrix}. \end{aligned} \quad (25)$$

To ensure that the time derivative of the Lyapunov function is strictly negative definite, i.e., $\dot{V}_i(\boldsymbol{\xi}_i(t)) < 0$, we need $\boldsymbol{\Phi}_i > 0$. That is, the matrix $\boldsymbol{\Phi}_i$ needs to strictly satisfy the positive definiteness, the sufficient condition of which can be

$$\begin{cases} K_{\alpha,i} > \theta_i, \\ K_{\beta,i} > \frac{K_{\alpha,i}^2 (\theta_i - K_{\alpha,i})}{4(K_{\alpha,i} - 2\theta_i)}, \end{cases} \quad (26)$$

which immediately results in the design constraints given in (15). Therefore, with the gains in (15), the trajectory of the sliding mode variable in (7) following the dynamics in (8) can converge to the origin in finite time. ■

It is remarked here that a suitable parameter θ_i involved in (26) is not unique and not exactly known in advance. Nevertheless, in

practice, in order to determine proper controller's gains based on (26) in the controller design stage, we can resort to simulation-based techniques and empirical analysis to incrementally adjust the values of the controller's gains or the parameter θ_i. The simulation-based tuning approach is of low complexity since the super-twisting SOSM controller needs only a small number of hyperparameters as shown in (26).

Let $V_i(\boldsymbol{s}_i(t))$ also denote $V_i(\boldsymbol{\xi}_i(t))$ in (18) where $\boldsymbol{s}_i(t) := [s_{1,i}(t), s_{2,i}(t)]^{\mathrm{T}}$ is the state vector of (16) for all $i \in \mathcal{I}_N$, and $\lambda_{\max}(\cdot)$ and $\lambda_{\min}(\cdot)$ denote the maximum and the minimum eigenvalues of an input matrix, respectively. Based on Theorem 1 and adopting the analysis logic in [45], [47], [49], we can also obtain the following theoretical result that provides an upper bound on the finite convergence time.

Corollary 1: For any $i \in \mathcal{I}_N$, given that the control law $u_i(t)$ follows (14) with the gains α_i and β_i satisfying (15), and $\boldsymbol{s}_i(0)$ is an initial state for (16), the time for the convergence of the sliding mode variable $s_i(t)$ in (7) following the dynamics in (8) to the origin is smaller than $T_i(\boldsymbol{s}_i(0))$, where $T_i(\boldsymbol{s}_i(0))$ is given as follows

$$\begin{cases} T\left(\boldsymbol{s}_i(0)\right) = \frac{2V_i^{\frac{1}{2}}(\boldsymbol{s}_i(0))}{\lambda(\boldsymbol{P}_i,\boldsymbol{\Phi}_i)}, \\ \lambda\left(\boldsymbol{P}_i,\boldsymbol{\Phi}_i\right) = \frac{(\lambda_{\min}(\boldsymbol{P}_i))^{\frac{1}{2}}\lambda_{\min}(\boldsymbol{\Phi}_i)}{\lambda_{\max}(\boldsymbol{P}_i)}. \end{cases} \tag{27}$$

Proof: According to (18), it always holds that

$$\lambda_{\min}\left(\boldsymbol{P}_i\right)\left\|\boldsymbol{\xi}_i(t)\right\|_2^2 \le V_i\left(\boldsymbol{s}_i(t)\right) \le \lambda_{\max}\left(\boldsymbol{P}_i\right)\left\|\boldsymbol{\xi}_i(t)\right\|_2^2 \tag{28}$$

for all $i \in \mathcal{I}_N$. Recalling (17), we can also have $\|\boldsymbol{\xi}_i(t)\|_2^2 = |s_{1,i}(t)| + s_{2,i}^2(t)$, which indicates $|s_{1,i}(t)| \le \|\boldsymbol{\xi}_i(t)\|_2^2$. Substituting (28) into this result can further yield

$$|s_{1,i}(t)|^{\frac{1}{2}} = |\xi_{1,i}(t)| \le \frac{V_i^{\frac{1}{2}}(\boldsymbol{s}_i(t))}{\left(\lambda_{\min}\left(\boldsymbol{P}_i\right)\right)^{\frac{1}{2}}}. \tag{29}$$

Besides, according to (24) and (28), it also holds that

$$\begin{aligned} \dot{V}_i(\boldsymbol{s}_i(t)) &\le -\frac{1}{|\xi_{1,i}(t)|}\lambda_{\min}\left(\boldsymbol{\Phi}_i\right)\left\|\boldsymbol{\xi}_i(t)\right\|_2^2 \\ &\le -\frac{1}{|\xi_{1,i}(t)|}\lambda_{\min}\left(\boldsymbol{\Phi}_i\right)\frac{V_i(\boldsymbol{s}_i(t))}{\lambda_{\max}\left(\boldsymbol{P}_i\right)} \end{aligned} \tag{30}$$

for all $i \in \mathcal{I}_N$. Combining (29) and (30) can lead to

$$\dot{V}_i(\boldsymbol{s}_i(t)) \le -\lambda\left(\boldsymbol{P}_i,\boldsymbol{\Phi}_i\right)V_i^{\frac{1}{2}}(\boldsymbol{s}(t)), i \in \mathcal{I}_N. \tag{31}$$

Note that for any $i \in \mathcal{I}_N$, the following differential align with an initial condition $V_i(0) \ge 0$

$$\dot{V}_i(t) = -\lambda\left(\boldsymbol{P}_i,\boldsymbol{\Phi}_i\right)V_i^{\frac{1}{2}}(t) \tag{32}$$

has a solution as

$$V_i(t) = \left(V_i^{\frac{1}{2}}(0) - \frac{\lambda\left(\boldsymbol{P}_i,\boldsymbol{\Phi}_i\right)t}{2}\right)^2. \tag{33}$$

Given $V_i(0) \ge V_i(\boldsymbol{s}_i(0))$, it always holds that $V_i(t) \ge V_i(\boldsymbol{s}_i(t))$. Therefore, $V_i(\boldsymbol{s}_i(t))$ along with $\boldsymbol{s}_i(t)$ can converge to zero at most after $2V_i^{\frac{1}{2}}(\boldsymbol{s}_i(0))/\lambda(\boldsymbol{P}_i,\boldsymbol{\Phi}_i)$ units of time. ■

IV. Nonlinear Disturbance Observer-Based Control Design

We remark that the practical implementation of the proposed control law (14) based on the super-twisting SOSM theory requires the prior knowledge on the upper bound of the composite term $\varphi(t,\boldsymbol{x}_i(t),\boldsymbol{\omega}_i(t))$ which involves the dynamics of both the state variable $\boldsymbol{x}_i(t)$ and the lumped disturbance $\boldsymbol{\omega}_i(t)$. However, it is impractical or even impossible to get the exact information about the dynamics of the disturbance term $\boldsymbol{\omega}_i(t)$. Thus, in the following section, motivated by the nonlinear disturbance observer (NDO) methodology [42]–[44], we would like to further design a NDO. Also different from the existing works [39]–[41], we design the NDO in the super-twisting SOSM format, termed super-twisting SOSMDO. The super-twisting SOSMDO is exploited to compensate the effect of the uncertain disturbances in the sliding mode dynamics.

Let $\varphi_i(t) := \varphi(t,\boldsymbol{x}_i(t),\boldsymbol{\omega}_i(t))$ for the simplicity of notations. According to (9), the composite term $\varphi_i(t)$ can be further decomposed into a known dynamics term $\varphi_i^*(t)$ that only involves the system state $\boldsymbol{x}_i(t)$ and an unknown disturbance term $\Delta\varphi_i(t)$ that depends on the disturbance $\boldsymbol{\omega}_i(t)$, i.e.,

$$\varphi_i(t) = \varphi_i^*(t) + \Delta\varphi_i(t), i \in \mathcal{I}_N, \tag{34}$$

where $\varphi_i^*(t) = \boldsymbol{k}_{i,1}\boldsymbol{x}_i(t) + c_i\dot{p}_{i,\text{target}}(t)$ and $\Delta\varphi_i(t) = \boldsymbol{k}_{i,2}\boldsymbol{\omega}_i(t)$. Now, (8) can be re-expressed in the following form

$$\dot{s}_i(t) = \varphi_i^*(t) + \Delta\varphi_i(t) - K_iu_i(t), i \in \mathcal{I}_N. \tag{35}$$

A. Super-Twisting SOSM-Based Disturbance Observation

To reconstruct the disturbance dynamics, we also resort to the super-twisting SOSM design methodology. To be specific, we introduce another auxiliary variable $g_i(t)$ as follows

$$\begin{cases} g_i(t) = s_i(t) + h_i(t), \\ \dot{h}_i(t) = -\varphi_i^*(t) + K_iu_i(t) - \phi_i(t), \end{cases} \tag{36}$$

for all $i \in \mathcal{I}_N$. By substituting (34) into (36), the time derivative of $g_i(t)$ can be derived as

$$\dot{g}_i(t) = \Delta\varphi_i(t) - \phi_i(t), i \in \mathcal{I}_N, \tag{37}$$

where $\phi_i(t)$ can be treated as the injection term of the proposed super-twisting SOSM-based disturbance observer in (37). Recalling that the disturbance $\boldsymbol{\omega}_i(t)$ and its first-order and second-order time derivatives are bounded as in (4), $\Delta\varphi_i(t)$ and its first-order time derivative $\Delta\dot{\varphi}_i(t)$ are bounded as well. We let L_i be an upper bound of $\Delta\dot{\varphi}_i(t)$, i.e., $|\Delta\dot{\varphi}_i(t)| \le L_i$. The injection term $\phi_i(t)$ can be written in the super twisting format with respect to $g_i(t)$

$$\begin{cases} \phi_i(t) = \gamma_{1,i}\left|g_i(t)\right|^{\frac{1}{2}}\text{sign}\left(g_i(t)\right) + y_i(t), \\ \dot{y}_i(t) = \gamma_{2,i}\text{sign}\left(g_i(t)\right), \end{cases} \tag{38}$$

for all $i \in \mathcal{I}_N$, where $\gamma_{1,i}$ and $\gamma_{2,i}$ are the observer's positive gains to be designed. Specifically, using the same logic presented in Section III and the results in (26), we can have the similar conditions for both $\gamma_{1,i}$ and $\gamma_{2,i}$, $i \in \mathcal{I}_N$, as follows.

Theorem 2: For any $i \in \mathcal{I}_N$, suppose that the disturbance term $\Delta\varphi_i(t)$ has the time derivative with a Lipschitz's constant

$L_i > 0$. Given that the estimate $\phi_i(t)$ follows (38) with the gains $\gamma_{1,i}$ and $\gamma_{2,i}$ satisfying

$$\begin{cases} \gamma_{1,i} > \sqrt{L_i}, \\ \gamma_{2,i} > \frac{\gamma_{1,i}^2\left(\sqrt{L_i}-\gamma_{1,i}\right)}{4\left(\gamma_{1,i}-2\sqrt{L_i}\right)}, \end{cases} \tag{39}$$

$g_i(t)$ in (36) following the dynamics in (37) can converge to the origin in finite time.

Proof: It is recognized that the super-twisting observer for the disturbance term $\Delta\varphi_i(t)$ in (38) has the same mathematical structure as that of the super-twisting SOSM controller as presented in (16). The goal of (38) is to make $\phi_i(t)$ converge to $\Delta\varphi_i(t)$, i.e., driving $g_i(t), \dot{g}_i(t) \to 0$. Besides, since the disturbance term $\Delta\varphi_i(t)$ has a time derivative with the Lipschitz's constant L_i and according to the first-order differentiator theory based on the sliding mode technique in [52] (see Proposition 2 and Theorem 2 in [52]), $|\Delta\varphi_i(t) - \phi_i(t)|$ in (37) can be bounded as the form $|\dot{g}_i(t)| = |\Delta\varphi_i(t) - \phi_i(t)| \le \sqrt{L_i}|g_i(t)|^{\frac{1}{2}}$ for some certain $L_i > 0$ and $i \in \mathcal{I}_N$. Thus, using the same logic of Theorem 1 and according to (26), we can replace the upper bound constant θ_i with the upper bound $\sqrt{L_i}$ to obtain the sufficient conditions in (39). ■

Besides, following the logic of Corollary 1, we can also obtain the following result.

Corollary 2: For any $i \in \mathcal{I}_N$, given that the estimate $\phi_i(t)$ follows (38) with the gains $\gamma_{1,i}$ and $\gamma_{2,i}$ satisfying (39), and $g_i(0)$ is an initial points for (36), the time for the convergence of the estimate $g_i(t)$ in (36) following the dynamics in (37) to the origin is smaller than $T_i(g_i(0))$, where $T_i(g_i(0))$ is given as follows

$$\begin{cases} T\left(g_i(0)\right) = \frac{2V_i^{\frac{1}{2}}\left(g_i(0)\right)}{\lambda\left(\boldsymbol{P}_{i,g},\boldsymbol{\Phi}_{i,g}\right)}, \\ \lambda\left(\boldsymbol{P}_{i,g},\boldsymbol{\Phi}_{i,g}\right) = \frac{\left(\lambda_{\min}\left(\boldsymbol{P}_{i,g}\right)\right)^{\frac{1}{2}}\lambda_{\min}\left(\boldsymbol{\Phi}_{i,g}\right)}{\lambda_{\max}\left(\boldsymbol{P}_{i,g}\right)}. \end{cases} \tag{40}$$

In (40), the matrix $\boldsymbol{P}_{i,g}$ is defined in the same form of (19) as follows

$$\boldsymbol{P}_{i,g} = \boldsymbol{P}\left(\gamma_{1,i},\gamma_{2,i}\right) = \frac{1}{2}\begin{bmatrix} 4\gamma_{2,i}+\gamma_{1,i}^2 & -\gamma_{1,i} \\ -\gamma_{1,i} & 2 \end{bmatrix}. \tag{41}$$

The matrix $\boldsymbol{\Phi}_{i,g}$ is defined like (25), i.e.,

$$\boldsymbol{\Phi}_{i,g} = -\left(\boldsymbol{Q}_{i,g}^{\mathrm{T}}\boldsymbol{P}_{i,g} + \boldsymbol{P}_{i,g}\boldsymbol{Q}_{i,g}\right) - 2\boldsymbol{P}_{i,g}\boldsymbol{\Lambda}_{i,g}, \tag{42}$$

where $\boldsymbol{Q}_{i,g}$ and $\boldsymbol{\Lambda}_{i,g}$ are formulated in the same form of (22) and (23), respectively, as follows

$$\begin{cases} \boldsymbol{Q}_{i,g} = \frac{1}{2}\begin{bmatrix} -\gamma_{1,i} & 1 \\ -2\gamma_{2,i} & 0 \end{bmatrix}, \\ \boldsymbol{\Lambda}_{i,g} = \frac{1}{2}\begin{bmatrix} \sqrt{L_i} & 0 \\ 0 & 0 \end{bmatrix}. \end{cases} \tag{43}$$

$V_i(g_i(t))$ is the Lyapunov function for the dynamics of $g_i(t)$, which can be given in the similar form of (18).

Proof: The proof logic of Corollary 2 is the same as that in Corollary 1, which is omitted here. ■

Theorem 2 as well as Corollary 2 characterizes the convergence condition for $g_i(t)$. Moreover, from (39) above, by letting $\sqrt{L_i} - \gamma_{1,i} = \gamma_{1,i} - 2\sqrt{L_i}$, i.e., $\gamma_{1,i} = 1.5\sqrt{L_i}$, the convergence condition leads to $\gamma_{2,i} > 0.5625L_i$. Therefore, by choosing $\gamma_{1,i} = 1.5\sqrt{L_i}$ and $\gamma_{2,i} = 2 \times (0.5625L_i) \approx 1.1L_i$, the convergence of $\dot{g}_i(t)$, $\dot{g}_i(t) \to 0$, can always be guaranteed. Then, an exact estimate of the disturbance $\Delta\varphi_i(t)$, denoted by $\widehat{\Delta\varphi}_i(t)$, can be set to

$$\widehat{\Delta\varphi}_i(t) = \phi_i(t) \to \Delta\varphi_i(t), i \in \mathcal{I}_N, \tag{44}$$

where $\phi_i(t)$ is obtained from the super-twisting dynamics (38) with $\gamma_{1,i} = 1.5\sqrt{L_i}$ and $\gamma_{2,i} = 1.1L_i$. In addition, it should be remarked that the upper bound parameter L_i related to the first derivative of the disturbance term $\Delta\varphi_i(t)$ can be properly estimated by empirical analysis or field measurements. However, in practice, an accurate estimation on the maximum value of $|\Delta\dot{\varphi}_i(t)|$ (i.e., the tight upper bound) is unnecessary, since there exist infinite number of positive constants that can be treated as an upper bound (i.e., the Lipschitz's constant) as long as they are larger than the maximum value of $|\Delta\dot{\varphi}_i(t)|$.

B. Platoon Controller Design Based on Super-Twisting SOSM Disturbance Observer (SOSMDO)

Using the super-twisting SOSM disturbance observer proposed above, we can further design a platoon controller $u_i(t)$ for each vehicle $i \in \mathcal{I}_N$, which is able to robustly asymptotically stabilize the sliding-mode variable $s_i(t)$ in the presence of an unknown but bounded disturbance $\Delta\varphi_i(t)$,

$$u_i(t) = \frac{1}{K_i}\left(\varphi_i^*(t) + \widehat{\Delta\varphi}_i(t) + \lambda_i s_i(t)\right), i \in \mathcal{I}_N, \tag{45}$$

where $\lambda_i > 0$ is a positive gain that should be sufficiently large to obtain a desired convergence rate of $s_i(t)$.

Theorem 3: For any $i \in \mathcal{I}_N$, given that the control law $u_i(t)$ follows (45) with a sufficiently large gain $\lambda_i > 0$, $s_i(t)$ in (7) following the dynamics in (8) can asymptotically converge to the origin as time increases.

Proof: By using the super-twisting nonlinear observer in (38), we can estimate the disturbance term as $\widehat{\Delta\varphi}_i(t)$ in (44). Then, the estimated disturbance $\widehat{\Delta\varphi}_i(t)$ is adopted in the control design in (45) to compensate the unknown disturbance effect. Thus, by substituting (45) into (35), the sliding-mode dynamics with the compensated disturbance is reduced to

$$\dot{s}_i(t) = -\frac{\lambda_i}{K_i}s_i(t), i \in \mathcal{I}_N, \tag{46}$$

which immediately indicates that $s_i(t)$ can be driven to asymptotically converge $s_i(t) \to 0$ as time increases. ■

We remark that the gain parameter λ_i should be properly selected in order to provide a desired convergence rate for $s_i(t) \to 0$ in an actual application situation. According to Theorem 3 above, a good choice is to let λ_i be one or two orders of magnitudes larger than K_i. Our proposed robust control implementation framework for each vehicle $i \in \mathcal{I}_N$ is shown in Fig. 1. Based on Theorem 3 and recalling (7), we can see that the designed controller $u_i(t)$ in (45) can robustly achieve platooning of the vehicles $i \in \mathcal{I}_N$ by driving both their position

and velocity tracking errors $e_{1,i}(t), e_{2,i}(t) \to 0$ in the presence of the unknown bounded disturbances $\boldsymbol{\omega}_i(t)$.

V. Performance Evaluation

A. Parameter Settings

To evaluate the performance of the proposed control design approach based on the super-twisting SOSMDO in Section IV, we consider a specific situation where $N = 5$ vehicles would like to form a platoon by tracking their individual reference trajectories determined by a virtual leader. The vehicle dynamics model is given in (2). For the demonstration purpose, the external disturbance $\boldsymbol{\omega}_i(t)$ in (2) is modeled as a scalar sinusoidal signal as follows

$$\boldsymbol{\omega}_i(t) = \eta_i \sin(2\pi f_i t), i = 1, 2, \ldots, N, \tag{47}$$

where f_i is the perturbation frequency in Hz and η_i is the perturbation amplitude. The coefficient matrix of $\boldsymbol{\omega}_i(t)$, $\boldsymbol{C}_i$, is specified as $\boldsymbol{C}_i = [1, 1, 1]^{\mathrm{T}}$, which indicates that the unknown disturbance term $\boldsymbol{\omega}_i(t)$ will appear in the position, velocity and acceleration state aligns of vehicle i. That is, we consider that the unknown disturbance will affect not only the acceleration profile but also both the position and velocity profiles of each individual vehicle. Besides, according to (6) and (7), the sliding-mode variable $s_i(t)$ can be re-arranged as

$$s_i(t) = c_i \Delta p_i(t) + (c_i b_{1,i} + 1)\Delta v_i(t) + b_{2,i}\Delta a_i(t) \tag{48}$$

for $i = 1, 2, \ldots, N$, where $\Delta p_i(t) = p_{i,\text{target}}(t) - p_i(t)$, $\Delta v_i(t) = v_{\text{target}} - v_i(t)$, and $\Delta a_i(t) = \dot{v}_{\text{target}} - \dot{v}_i(t)$. The coefficients c_i, $b_{1,i}$, and $b_{2,i}$ need to be properly selected to make the corresponding characteristic polynomial $P_i(\sigma) = b_{2,i}\sigma^2 + (c_i b_{1,i} + 1)\sigma + c_i$ Hurwitz, where σ is used to denote the Laplace variable here. Therefore, the eigenvalue of $P_i(\sigma) = 0$ should have a negative real part. In our simulations, we specify a positive $\mu_i > 0$ and then let $b_{2,i} = 1$ while $c_i = \mu_i^2$ and $(c_i b_{1,i} + 1) = 2\mu_i$. In this way, the polynomial becomes $P_i(\sigma) = (\sigma + \mu_i)^2$, which is always Hurwitz stable.

In addition, from (9) and (34), it is seen that $\Delta\varphi_i(t) = \boldsymbol{k}_{i,2}\boldsymbol{\omega}_i(t)$. Hence, given (47), the upper bound of the time-derivative of $\Delta\varphi_i(t)$, L_i, can be determined as $L_i = \sup_{\forall t}|\boldsymbol{k}_{i,2}\boldsymbol{C}_i\dot{\boldsymbol{\omega}}_i(t)| = 2\pi f_i \eta_i |\boldsymbol{k}_{i,2}\boldsymbol{C}_i|$ in our simulations. The modeling parameters of the super-twisting SOSM-based and the super-twisting SOSMDO-based controllers are summarized in Table I. The settings in Table I will be adopted throughout the simulation experiments unless otherwise stated.

TABLE I
Parameter Settings

Vehicle dynamics model		
N	Platooning vehicle number	5
v_{target}	Desired steady velocity (km/h)	50
κ	Ratio of active control input	90%
τ	Actuation time lag for control input (s)	0.1
Δt	Constant time headway (s)	1.28
External disturbance		
$\boldsymbol{C}_i$	Coefficient matrix of disturbance	$[1, 1, 1]^{\mathrm{T}}$
η_i	Disturbance amplitude	0.5
f_i	Disturbance frequency (Hz)	0.1
Sliding-mode variable		
c_i	Weight for the position tracking error	μ_i^2
$b_{1,i}$	Weight for the velocity tracking error	$\frac{2\mu_i - 1}{c_i}$
$b_{2,i}$	Weight for the acceleration tracking error	1
μ_i	Positive constant	1.5
Super-twisting SOSM-based platoon controller		
α_i	Control gain	1.5
β_i	Control gain	0.1
Super-twisting SOSMDO-based platoon controller		
$\gamma_{1,i}$	Control gain	$1.5\sqrt{L_i}$
$\gamma_{2,i}$	Control gain	$1.1L_i$
λ_i	Control gain	5×10^2
L_i	Upper bound of $\Delta\dot{\varphi}_i(t)$	$2\pi f_i \eta_i \lvert\boldsymbol{k}_{i,2}\boldsymbol{C}_i\rvert$

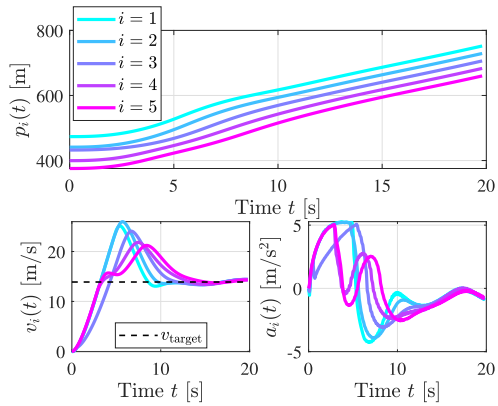

Fig. 2. The longitudinal positions, velocities, and accelerations of $N = 5$ platooning vehicles adopting the super-twisting SOSM controller.

B. Validation of Robustness in Platooning

The robustness of the proposed platoon controllers based on both the super-twisting SOSM and the super-twisting SOSMDO is illustrated in Figs. 2 to 9. In order to test the control performance under different dynamics stages of the platooning vehicles, including an acceleration stage, a deceleration stage and a stage of stabilization around the equilibrium velocity, we initialize the vehicles' longitudinal velocities and accelerations to zero at the initial time. Besides, the longitudinal inter-vehicle spacing is randomly generated by the perturbation of the equilibrium. Fig. 2 shows the profiles of their longitudinal positions, velocities, and accelerations over time under the super-twisting SOSM platoon controller. It is seen that all the vehicles increase their velocities during the first 5 seconds to adjust their inter-spacing and avoid chain collisions. After about 15 seconds, the vehicles can almost reach the equilibrium state in which their longitudinal velocities approximate the desired level and their inter-distances are almost identical. Figs. 3 and 4 detail the profiles of the inter-vehicle spacing and the velocity deviation between any two successive vehicles, respectively. It is observed that all the platooning vehicles can track the reference velocity when arriving at the equilibrium state, and they are also able to reach the identical inter-spacing without chain collisions even under external disturbances. Specifically, from Fig. 3, the averaged absolute error of the vehicles' inter-spacing is about $0.31\,\mathrm{m}$ over the last 5 seconds, while the absolute error of their velocity differences is about $0.11\,\mathrm{m/s}$ on average. Fig. 5

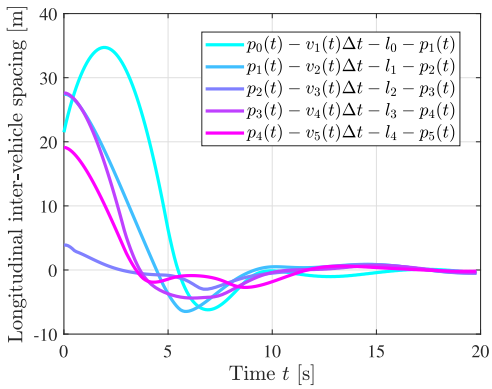

Fig. 3. The longitudinal inter-vehicle spacing of $N = 5$ platooning vehicles adopting the super-twisting SOSM controller.

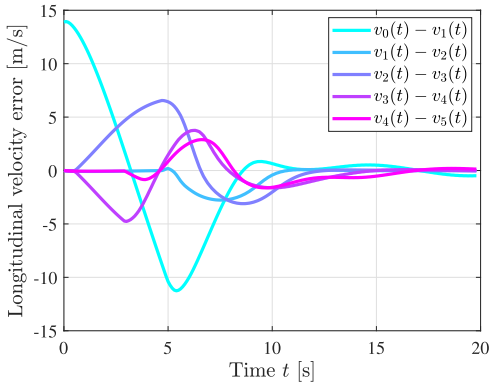

Fig. 4. The longitudinal velocity deviations of $N = 5$ platooning vehicles adopting the super-twisting SOSM controller.

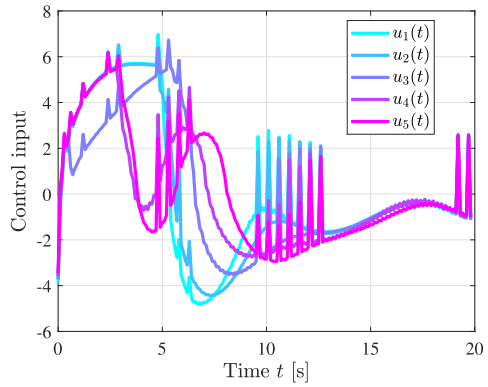

Fig. 5. The control inputs of $N = 5$ platooning vehicles adopting the super-twisting SOSM controller.

illustrates that all the vehicles can behave in the same control manner when they reach the equilibrium after 15 seconds.

Similarly, as depicted in Figs. 6 to 9, the simulation results also validate the robustness of the super-twisting SOSMDO controller in the presence of external disturbances. From Fig. 6, it can be observed that the disturbance observer-based platoon controller can drive the vehicles to achieve almost the same profile in both the time and spatial domains when they arrive at

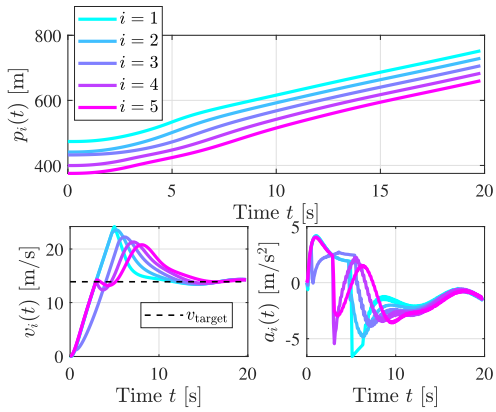

Fig. 6. The longitudinal positions, velocities, and accelerations of $N = 5$ platooning vehicles adopting the super-twisting SOSMDO-based controller.

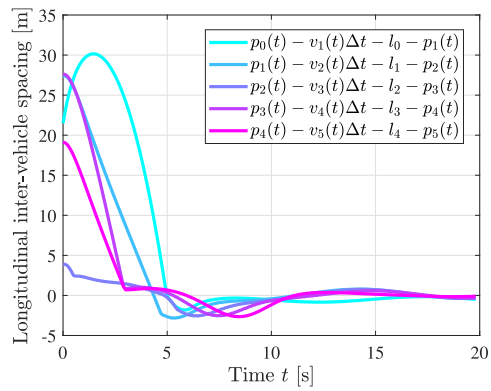

Fig. 7. The longitudinal inter-vehicle spacing of $N = 5$ platooning vehicles adopting the super-twisting SOSMDO-based controller.

the equilibrium state after about 15 seconds. In particular, the averaged absolute error of the vehicles' inter-spacing is about $0.27\,\mathrm{m}$ over the last 5 seconds in Fig. 7, and the averaged absolute error of their velocity differences is about $0.10\,\mathrm{m/s}$. When compared to the results of the super-twisting SOSM platoon controller in Figs. 3 to 4, the averaged inter-vehicle spacing error in the stabilization of the platooning equilibrium under the super-twisting SOSMDO platoon controller is reduced by about 13.19%, while the averaged velocity tracking error is reduced by about 14.01%. The results confirm that the super-twisting SOSMDO platoon controller can achieve better platooning performance than the super-twisting SOSM. As depicted in Fig. 9, since the unknown disturbance is estimated and compensated in the control signal, the amplitude of the control output by the super-twisting SOSMDO platoon controller is larger than that in Fig. 5. However, Fig. 9 shows that the vehicles under the super-twisting SOSMDO platoon controller can achieve the same control profile more quickly and a better tracking accuracy than the super-twisting SOSM platoon controller. Besides, from either Figs. 3 and 4 or Figs. 7 and 8, the platooning errors are always bounded and sufficiently small. In summary, the above results confirm that both the designed platoon controllers can asymptotically and robustly achieve the stabilization of the

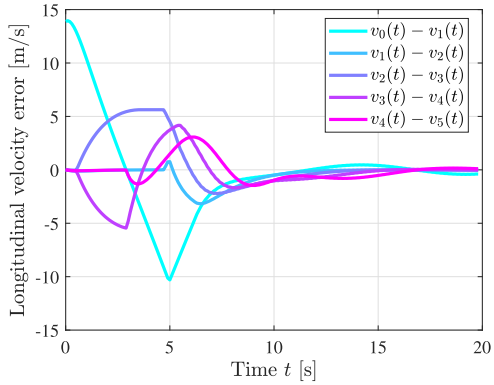

Fig. 8. The longitudinal velocity deviations of $N = 5$ platooning vehicles adopting the super-twisting SOSMDO-based controller.

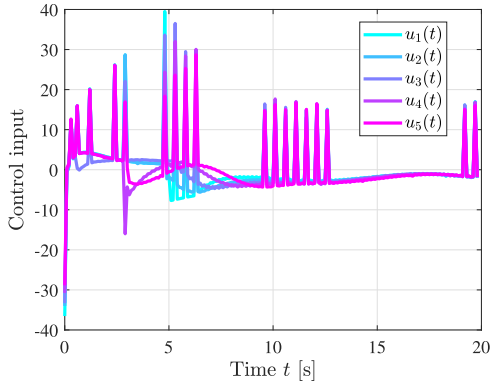

Fig. 9. The control inputs of $N = 5$ platooning vehicles adopting the super-twisting SOSMDO-based controller.

platooning equilibrium in finite time, which is in consistence with Theorems 1 to 3.

C. Performance Comparison

To further demonstrate the advantage of the designed platoon controllers, we also conduct a series of simulations and compare the performance of both the super-twisting SOSM and the super-twisting SOSMDO platoon controllers with the conventional model predictive control (MPC)-based method under different disturbances. Here, the design parameters for both the designed platoon controllers use the values in Table I. To simulate different perturbation patterns, we vary the amplitude and frequency of the disturbance in (47), η_i and f_i for $i = 1, 2, \ldots, N$. The disturbance term $\boldsymbol{\omega}_i(t)$ varying over time is illustrated with different η_i and f_i in Fig. 10.

In addition, for performance comparison, we also introduce the following two key performance indicators (KPIs):

i) The average absolute error of the longitudinal inter-vehicle spacing during the last ΔT seconds, which is denoted by Avg. $|\Delta p|$ and can be calculated by

$$\text{Avg.}|\Delta p| = \frac{1}{N}\sum_{i=1}^{N}\frac{\int_{T_f-\Delta T}^{T_f}|p_{i-1}(t)-v_i\Delta t-l_{i-1}-p_i(t)|dt}{\Delta T}, \tag{49}$$

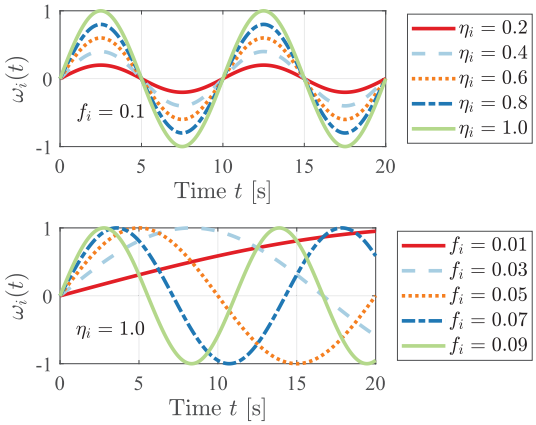

Fig. 10. The different disturbances adopted for the performance comparison.

where T_f denotes the end time of a simulation period.

ii) The average absolute error of the longitudinal velocity deviation during the last ΔT seconds, which is denoted by Avg. $|\Delta v|$ and is calculated in a similar way as (49)

$$\text{Avg.}|\Delta v| = \frac{1}{N}\sum_{i=1}^{N}\frac{\int_{T_f-\Delta T}^{T_f}|v_{i-1}(t)-v_i(t)|\,dt}{\Delta T}. \tag{50}$$

Avg. $|\Delta p|$ and Avg. $|\Delta v|$ comprehensively reflect the stabilization performance of the platoon in terms of inter-vehicle spacing and velocity tracking, respectively. Besides, Avg. $|\Delta p|$ is in meters and Avg. $|\Delta v|$ is in meters per second.

1) Effect of Different Disturbance Amplitudes: In Figs. 11 and 12, we set the unknown disturbance frequency as $f_i = 0.1\,\text{Hz}$ for $i = 1, 2, \ldots, N$ and conduct the performance comparison under different disturbance amplitudes $\eta_i \in \{0.2, 0.4, 0.6, 0.8, 1.0\}$. From Fig. 11, it is clear that a larger disturbance amplitude can lead to a larger convergence error in the inter-vehicle spacing between any two successive platooning vehicles. Nevertheless, our designed super-twisting SOSM and SOSMDO platoon controllers can ensure the convergence of the inter-vehicle spacing $(p_{i-1}(t) - v_i(t)\Delta t - l_{i-1} - p_i(t))$ and stabilize the inter-vehicle spacing around the desired level, even when increasing the unknown disturbance amplitude. By comparison, the inter-vehicle spacing under the conventional MPC cannot stabilize the platooning of the vehicles when the disturbance amplitude is large. In Fig. 11, a larger disturbance results in a larger perturbation in the inter-vehicle spacing under the conventional MPC, while our controllers can still achieve the stabilization of the equilibrium state.

Fig. 12 also shows the robustness of our designed controllers in terms of velocity tracking. It can be observed that the velocity difference between any two successive platooning vehicles at the equilibrium point, $(v_{i-1}(t) - v_i(t))$ for $i = 1, 2, \ldots, N$, is less sensitive to the variation of the disturbance amplitude, when the vehicles use the super-twisting SOSM and the super-twisting SOSMDO controllers. However, with the conventional MPC, the vehicles cannot accurately track the reference velocity and they will experience a stronger perturbation in the velocity tracking error between adjacent vehicles when the unknown

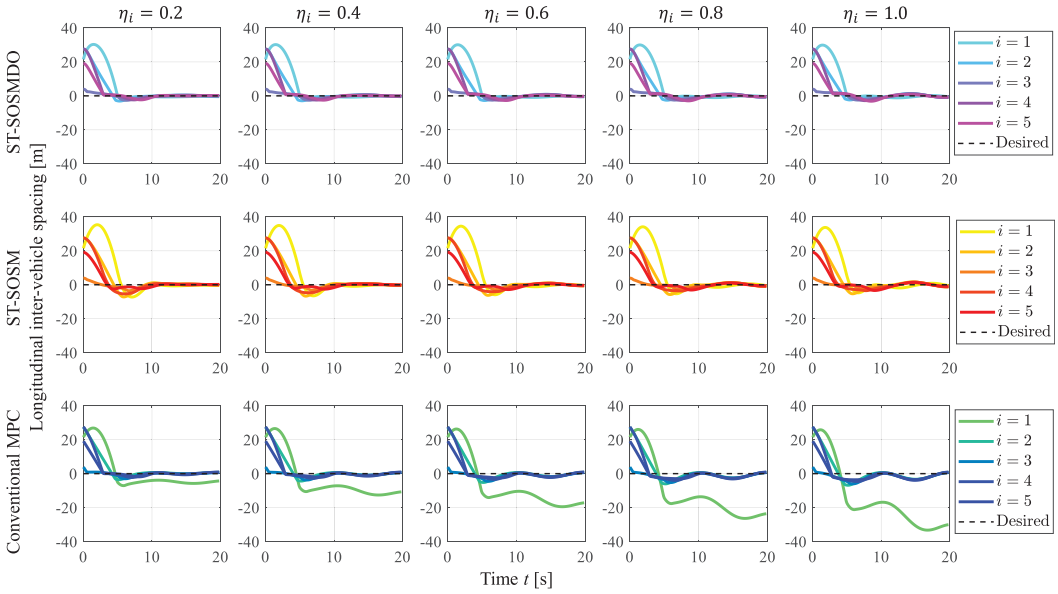

Fig. 11. The longitudinal inter-vehicle spacing of $N = 5$ platooning vehicles adopting different controllers under different disturbance amplitudes.

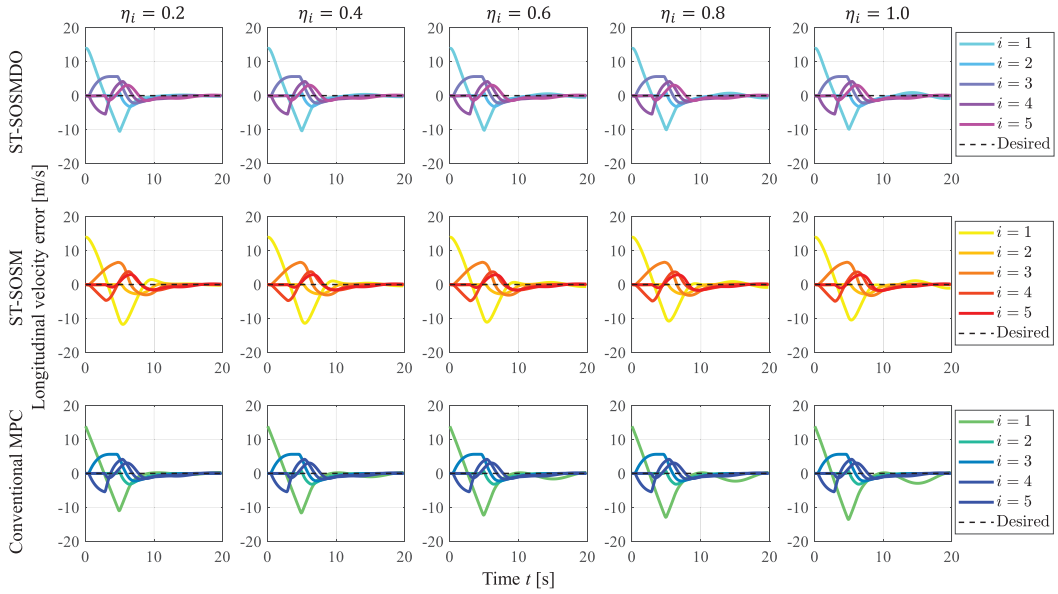

Fig. 12. The longitudinal velocity deviations of $N = 5$ platooning vehicles adopting different controllers under different disturbance amplitudes.

disturbance becomes larger. In Table II, we summarize the KPIs of the compared control methods under different disturbance amplitudes, in which the size of the observation time window, ΔT, is set to 10 seconds. From Table II, it can be seen that our proposed method, ST-SOSMDO, can achieve the smallest inter-vehicle spacing error and the smallest velocity tracking error. In particular, when the disturbance amplitude is relatively large, i.e., $\eta_i = 1.0$, the average absolute error of the inter-vehicle spacing during the last 10 seconds is only about $0.6620\,\mathrm{m}$ under our ST-SOSMDO method, which is one order of magnitude smaller than that (about $6.6924\,\mathrm{m}$) under the MPC method. The average absolute error of the velocity deviation is about $0.3227\,\mathrm{m/s}$ under our ST-SOSMDO, which is about 32.90% lower than that (about $0.4809\,\mathrm{m/s}$) under the MPC. As shown in Table II, when compared to the ST-SOSM method based on the second-order sliding mode theory, the ST-SOSMDO method can achieve better tracking and stabilization performance, which reduces the inter-spacing error by about 19.30% and the velocity tracking error by about 15.44% on average.

2) Effect of Different Disturbance Frequencies: Figs. 13 and 14 compare the control performance under different disturbance frequencies. In these two figures, we fix the disturbance amplitude at $\eta_i = 1.0$ and vary the frequency $f_i \in \{0.01, 0.03, 0.05, 0.07, 0.09\}\,(\mathrm{Hz})$ for $i = 1, 2, \ldots, N$. From Fig. 13, we can see that the disturbance with a higher frequency has a slight influence on the stabilization of the platooning

TABLE II
PERFORMANCE COMPARISON UNDER DIFFERENT DISTURBANCE AMPLITUDES

	$\eta_i = 0.2$		$\eta_i = 0.4$		$\eta_i = 0.6$		$\eta_i = 0.8$		$\eta_i = 1.0$	
Method & KPI	Avg. $\lvert\Delta p\rvert$	Avg. $\lvert\Delta v\rvert$	Avg. $\lvert\Delta p\rvert$	Avg. $\lvert\Delta v\rvert$	Avg. $\lvert\Delta p\rvert$	Avg. $\lvert\Delta v\rvert$	Avg. $\lvert\Delta p\rvert$	Avg. $\lvert\Delta v\rvert$	Avg. $\lvert\Delta p\rvert$	Avg. $\lvert\Delta v\rvert$
ST-SOSMDO	0.2493	0.2328	0.3165	0.2553	0.4248	0.2778	0.5386	0.3002	0.6620	0.3227
ST-SOSM	0.3311	0.3146	0.3643	0.3113	0.4945	0.3138	0.6712	0.3322	0.8805	0.3672
MPC	1.2410	0.2432	2.5212	0.2968	3.8919	0.3564	5.2856	0.4183	6.6924	0.4809

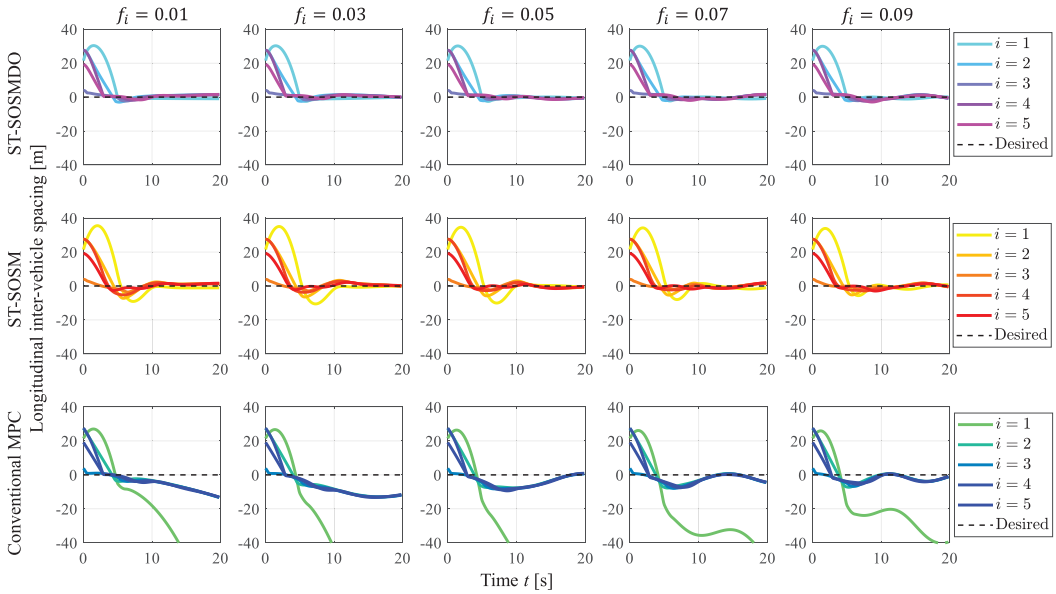

Fig. 13. The longitudinal inter-vehicle spacing of $N = 5$ platooning vehicles adopting different controllers under different disturbance frequencies.

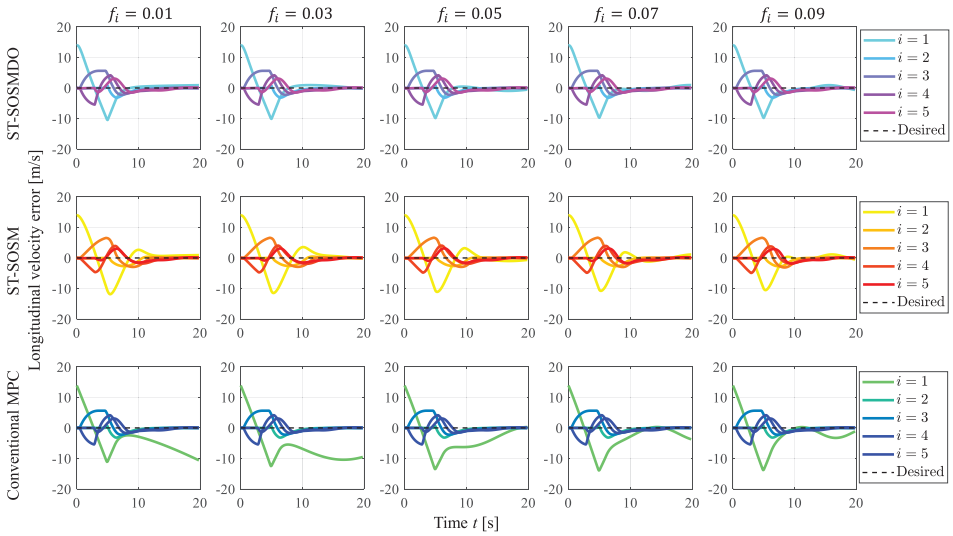

Fig. 14. The longitudinal velocity deviations of $N = 5$ platooning vehicles adopting different controllers under different disturbance frequencies.

equilibrium by using our designed controllers. In contrast, the inter-vehicle spacing of the platoon cannot be stabilized around the desired level under the conventional MPC. In particular, with a relatively small disturbance frequency, e.g., $f_i = 0.01$ Hz, the perturbation in the inter-vehicle spacing is larger under the conventional MPC. This indicates that the conventional MPC is disturbance-unstable. The main reason is that the disturbance is monotonously increasing over the finite time horizon $[0, 20]$ (s) when its frequency is low (See Fig. 10). However, both our super-twisting SOSM and SOSMDO controllers still guarantee the platooning stability in the presence of the low-frequency uncertain disturbance.

Besides, Fig. 14 demonstrates the profiles of the velocity differences between adjacent vehicles under different controls.

TABLE III
PERFORMANCE COMPARISON UNDER DIFFERENT DISTURBANCE FREQUENCIES

	$f_i = 0.01$		$f_i = 0.03$		$f_i = 0.05$		$f_i = 0.07$		$f_i = 0.09$	
Method & KPI	Avg. $\lvert\Delta p_i\rvert$	Avg. $\lvert\Delta v_i\rvert$	Avg. $\lvert\Delta p_i\rvert$	Avg. $\lvert\Delta v_i\rvert$	Avg. $\lvert\Delta p_i\rvert$	Avg. $\lvert\Delta v_i\rvert$	Avg. $\lvert\Delta p_i\rvert$	Avg. $\lvert\Delta v_i\rvert$	Avg. $\lvert\Delta p_i\rvert$	Avg. $\lvert\Delta v_i\rvert$
ST-SOSMDO	0.9984	0.3534	0.7472	0.3219	0.5821	0.3267	0.8474	0.3393	0.7084	0.3212
ST-SOSM	1.2201	0.5216	1.0515	0.5378	0.8621	0.4817	0.9560	0.3950	0.8678	0.3586
MPC	16.5246	1.4798	27.9721	2.0857	15.2665	0.8192	8.4550	0.4618	7.5556	0.5378

It is seen that our designed controllers can enable the vehicles to track the desired velocity with a sufficiently good accuracy and stabilize the platoon at the equilibrium under different disturbance frequencies. With a low frequency, for instance, $f_i = 0.01$ Hz or $f_i = 0.03$ Hz, the conventional MPC fails to stabilize the tracking of the reference velocity. The platoon with the conventional MPC experiences an obvious perturbation in the velocity tracking. By comparison, the super-twisting SOSM and SOSMDO platoon controllers can robustly track the desired velocity and guarantee the stability of the vehicle platooning at the equilibrium velocity. In Table III, we additionally provide the KPIs of the compared methods under different disturbance frequencies. We can observe that our ST-SOSMDO method achieves the best tracking and stabilization performance among these compared methods. Our method can reduce Avg. $|\Delta p|$ by about 21.86% and Avg. $|\Delta v|$ by about 25.82% on average when compared to the ST-SOSM. Besides, Avg. $|\Delta p|$ and Avg. $|\Delta v|$ of our ST-SOSMDO are about 93.62% and 57.52% lower than the corresponding KPIs of the MPC method on average, respectively.

3) Effect of Different Platoon Sizes: We additionally conduct simulations to show the effect of the platoon size (i.e., the number of vehicles in the platoon) and thus to further verify the superior performance of our proposed control method. In the simulations, in order to simulate more complicated and heterogeneous disturbances of individual vehicles, we consider the following disturbance signal

$$\boldsymbol{\omega}_i(t) = \Delta\eta_i + \eta_i \sin(2\pi f_i t), \tag{51}$$

where $\Delta\eta_i$ is a constant disturbance term and $\eta_i \sin(2\pi f_i t)$ is a time-varying disturbance term. For each vehicle $i = 1, 2, \ldots, N$, $\Delta\eta_i$ and η_i are randomly generated within [0.1,1.0], i.e., $\Delta\eta_i, \eta_i \sim U[0.1, 1.0]$, while f_i is randomly generated within [1,10], i.e., $f_i \sim U[1, 10]$. In this way, the external disturbance experienced by a vehicle, $\boldsymbol{\omega}_i(t)$, will be different from each other in the simulation experiment.

To illustrate the comprehensive performance of our proposed ST-SOSMDO method in a large-scale platooning scenario, we set the vehicle number to $N = 50$. The initial velocity of each vehicle is generated by the 20% perturbation of the desired velocity. The simulation results are given in Figs. 15, 16 and 17. In Fig. 15, the position profile of the platoon shows that all the vehicles can asymptotically reach their stable platooning trajectories. Fig. 15 also demonstrates that the vehicles can stably track the desired velocity after an acceleration stage or a deceleration stage. The inter-vehicle spacing error is shown in Fig. 16. It can be seen that the fluctuation pattern of each

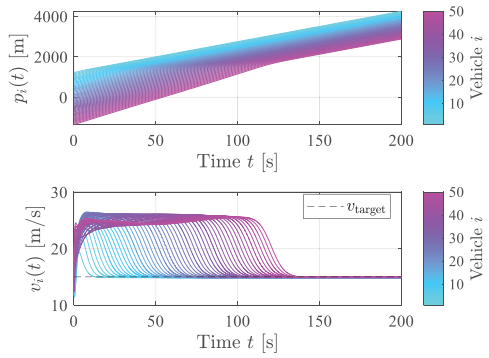

Fig. 15. The longitudinal positions and velocities of $N = 50$ platooning vehicles adopting the super-twisting SOSMDO-based controller.

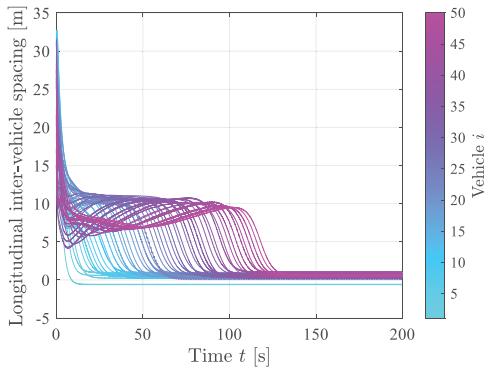

Fig. 16. The longitudinal inter-vehicle spacing of $N = 50$ platooning vehicles adopting the super-twisting SOSMDO-based controller.

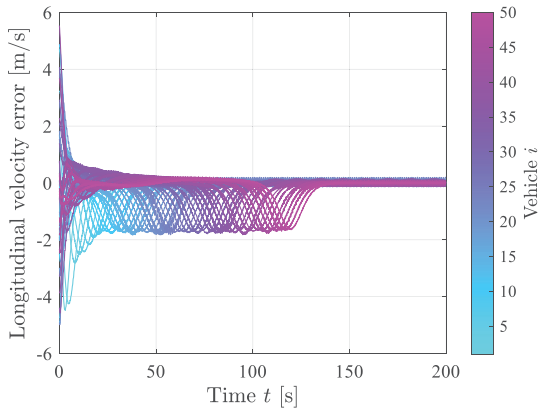

Fig. 17. The longitudinal velocity deviations of $N = 50$ platooning vehicles adopting the super-twisting SOSMDO-based controller.

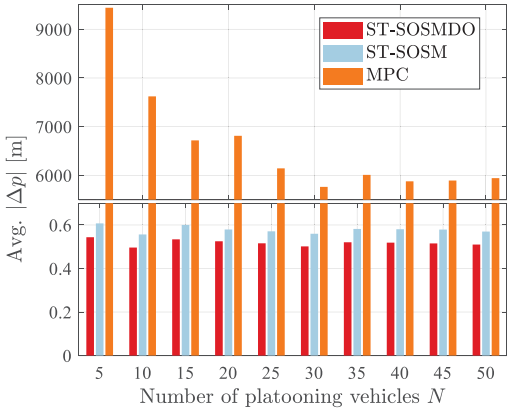

Fig. 18. The average absolute error of the inter-vehicle spacing under different platooning vehicle numbers.

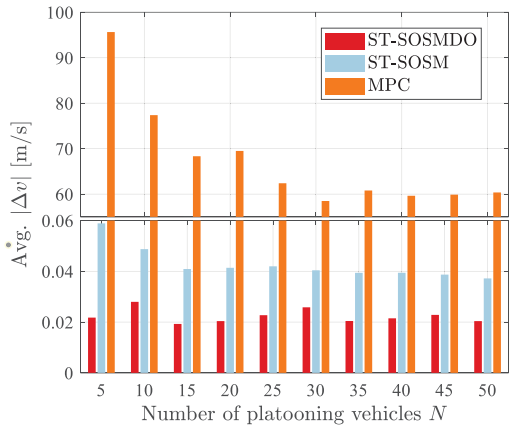

Fig. 19. The average absolute error of the velocity deviation under different platooning vehicle numbers.

vehicle's curve is different from each other, since the heterogeneity in the individual disturbance term is considered in the simulation scenario. Nevertheless, the inter-vehicle spacing errors of all the vehicles asymptotically converge to the neighborhood of the zero point during the last 50 seconds. Similarly, it is observed from Fig. 17 that the vehicles' velocity deviations have different fluctuations but can also converge asymptotically.

In the following, we compare the proposed ST-SOSMDO method with the ST-SOSM method and the conventional MPC method under different platoon sizes. The vehicle number is set as $N \in \{5, 10, 15, \ldots, 50\}$. The velocities and positions of all the vehicles are also initialized by the random perturbation of the equilibrium state as aforementioned. Figs. 18 and 19 demonstrate the simulation results in terms of the KPIs. From these two figures, it is seen that the inter-vehicle spacing and velocity tracking errors of the conventional MPC method are much higher than those of the other two methods. This fact implies that the conventional MPC fails in stably controlling the vehicle platoon since it cannot handle the external uncertain disturbance of each vehicle. In Fig. 18, the inter-vehicle spacing error of our proposed ST-SOSMDO method under different platoon sizes is about $0.5181\,\mathrm{m}$ on average, which is 10.43% lower than that ($0.5784\,\mathrm{m}$) of the ST-SOSM method. In Fig. 19, our ST-SOSMDO method has the velocity tracking error of about $0.0223\,\mathrm{m/s}$ on average, which is 47.76% lower than that ($0.0427\,\mathrm{m/s}$) of the ST-SOSM method. Moreover, it is also observed that both the KPIs of the robust control methods are not sensitive to the variation of the platoon size. That is, increasing the platoon size does not obviously increase the inter-vehicle spacing and velocity tracking errors under the ST-SOSMDO and the ST-SOSM methods. The main reason is that the robust control methods can benefit from their decentralized implementation.

VI. Conclusion and Future Work

In this study, we have investigated the longitudinal platooning control of vehicles in the presence of unknown but bounded external disturbances. The platooning goal is to drive the vehicles to track a desired velocity profile meanwhile keeping a constant space headway for the sake of collision avoidance. To this end, we have proposed a decentralized robust control approach with a super-twisting second-order sliding mode disturbance observer (SOSMDO). We have also proved the asymptotic stability of the super-twisting SOSMDO platoon controller and its robustness to the external uncertain disturbances. Extensive simulations have been conducted and the simulation results have demonstrated that the super-twisting SOSMDO can improve performance in both the inter-vehicle spacing and the velocity tracking accuracy when compared to the conventional MPC and the super-twisting SOSM approach. As our future work, we will extend the proposed robust platoon control approach to mixed traffic flows, in which the autonomous vehicles and the human-driven vehicles are considered to cooperate to form a platoon. Besides, we would also like to consider higher heterogeneity in the uncertain disturbance reconstruction, and conduct performance comparison with some other robust methodologies (e.g., the H-infinity method and gain-scheduled methods) under more complicated application scenarios.

References

[1] Z. Wang, Y. Bian, S. E. Shladover, G. Wu, S. E. Li, and M. J. Barth, "A survey on cooperative longitudinal motion control of multiple connected and automated vehicles," *IEEE Intell. Transp. Syst. Mag.*, vol. 12, no. 1, pp. 4–24, 2020.

[2] S. E. Li *et al.*, "Dynamical modeling and distributed control of connected and automated vehicles: Challenges and opportunities," *IEEE Intell. Transp. Syst. Mag.*, vol. 9, no. 3, pp. 46–58, 2017.

[3] D. Jia, K. Lu, J. Wang, X. Zhang, and X. Shen, "A survey on platoon-based vehicular cyber-physical systems," *IEEE Commun. Surv. Tut.*, vol. 18, no. 1, pp. 263–284, Jan.–Mar. 2016.

[4] J. Zhou, D. Tian, Y. Wang, Z. Sheng, X. Duan, and V. C. Leung, "Reliability-optimal cooperative communication and computing in connected vehicle systems," *IEEE Trans. Mobile Comput.*, vol. 19, no. 5, pp. 1216–1232, May 2020.

[5] J. Zhou, D. Tian, Y. Wang, Z. Sheng, X. Duan, and V. C. M. Leung, "Reliability-oriented optimization of computation offloading for cooperative vehicle-infrastructure systems," *IEEE Signal Process. Lett.*, vol. 26, no. 1, pp. 104–108, Jan. 2019.

[6] D. Swaroop and J. K. Hedrick, "Constant spacing strategies for platooning in automated highway systems," *J. Dynamic Syst., Measurement, Control*, vol. 121, no. 3, pp. 462–470, 1999. [Online]. Available: https://doi.org/10.1115/1.2802497

[7] P. Ioannou and C. Chien, "Autonomous intelligent cruise control," *IEEE Trans. Veh. Technol.*, vol. 42, no. 4, pp. 657–672, Nov. 1993.

[8] P. Y. Li and A. Shrivastava, "Traffic flow stability induced by constant time headway policy for adaptive cruise control vehicles," *Transp. Res. Part C: Emerg. Technol.*, vol. 10, no. 4, pp. 275–301, 2002. [Online]. Available: https://www.sciencedirect.com/science/article/pii/S0968090X02000049

[9] F. Ma *et al.*, "Distributed control of cooperative vehicular platoon with nonideal communication condition," *IEEE Trans. Veh. Technol.*, vol. 69, no. 8, pp. 8207–8220, Aug. 2020.

[10] H. Xing, J. Ploeg, and H. Nijmeijer, "Compensation of communication delays in a cooperative ACC system," *IEEE Trans. Veh. Technol.*, vol. 69, no. 2, pp. 1177–1189, Feb. 2020.

[11] Y. Zhu, D. Zhao, and H. He, "Synthesis of cooperative adaptive cruise control with feedforward strategies," *IEEE Trans. Veh. Technol.*, vol. 69, no. 4, pp. 3615–3627, Apr. 2020.

[12] M. Wang, "Infrastructure assisted adaptive driving to stabilise heterogeneous vehicle strings," *Transp. Res. Part C: Emerg. Technol.*, vol. 91, pp. 276–295, 2018. [Online]. Available: https://www.sciencedirect.com/science/article/pii/S0968090X18304674

[13] G. J. L. Naus, R. P. A. Vugts, J. Ploeg, M. J. G. van de Molengraft, and M. Steinbuch, "String-stable CACC design and experimental validation: A frequency-domain approach," *IEEE Trans. Veh. Technol.*, vol. 59, no. 9, pp. 4268–4279, Nov. 2010.

[14] Y. Zhou, S. Ahn, M. Chitturi, and D. A. Noyce, "Rolling horizon stochastic optimal control strategy for ACC and CACC under uncertainty," *Transp. Res. Part C: Emerg. Technol.*, vol. 83, pp. 61–76, 2017. [Online]. Available: https://www.sciencedirect.com/science/article/pii/S0968090X17301997

[15] Y. Zhou and S. Ahn, "Robust local and string stability for a decentralized car following control strategy for connected automated vehicles," *Transp. Res. Part B: Methodological*, vol. 125, pp. 175–196, 2019. [Online]. Available: https://www.sciencedirect.com/science/article/pii/S0191261518306234

[16] Y. Zhu, D. Zhao, and Z. Zhong, "Adaptive optimal control of heterogeneous CACC system with uncertain dynamics," *IEEE Trans. Control Syst. Technol.*, vol. 27, no. 4, pp. 1772–1779, Jul. 2019.

[17] S. E. Li, X. Zhang, R. Li, Z. Wang, H. Chen, and Z. Xin, "Optimal periodic control of connected multiple vehicles with heterogeneous dynamics and guaranteed bounded stability," *IEEE Intell. Transp. Syst. Mag.*, vol. 12, no. 4, pp. 110–124, 2020.

[18] K. Li, F. Gao, S. Li, Y. Zheng, and H. Gao, "Robust cooperation of connected vehicle systems with eigenvalue-bounded interaction topologies in the presence of uncertain dynamics," *Front. Mech. Eng.*, vol. 13, pp. 1–14, Dec. 2017.

[19] K. Li, S. E. Li, F. Gao, Z. Lin, J. Li, and Q. Sun, "Robust distributed consensus control of uncertain multiagents interacted by eigenvalue-bounded topologies," *IEEE Internet Things J.*, vol. 7, no. 5, pp. 3790–3798, May 2020.

[20] S. E. Li, X. Qin, Y. Zheng, J. Wang, K. Li, and H. Zhang, "Distributed platoon control under topologies with complex eigenvalues: Stability analysis and controller synthesis," *IEEE Trans. Control Syst. Technol.*, vol. 27, no. 1, pp. 206–220, Jan. 2019.

[21] S. E. Li, F. Gao, K. Li, L.-Y. Wang, K. You, and D. Cao, "Robust longitudinal control of multi-vehicle systems'a distributed h-infinity method," *IEEE Trans. Intell. Transp. Syst.*, vol. 19, no. 9, pp. 2779–2788, Sep. 2018.

[22] Y. Zheng, S. E. Li, K. Li, and W. Ren, "Platooning of connected vehicles with undirected topologies: Robustness analysis and distributed h-infinity controller synthesis," *IEEE Trans. Intell. Transp. Syst.*, vol. 19, no. 5, pp. 1353–1364, May 2018.

[23] Y. Zhou, S. Ahn, M. Wang, and S. Hoogendoorn, "Stabilizing mixed vehicular platoons with connected automated vehicles: An h-infinity approach," *Transp. Res. Part B: Methodological*, vol. 132, pp. 152–170, 2020. [Online]. Available: https://www.sciencedirect.com/science/article/pii/S0191261518311482

[24] M. Wang, W. Daamen, S. P. Hoogendoorn, and B. van Arem, "Rolling horizon control framework for driver assistance systems. part i: Mathematical formulation and non-cooperative systems," *Transp. Res. Part C: Emerg. Technol.*, vol. 40, pp. 271–289, 2014. [Online]. Available: https://www.sciencedirect.com/science/article/pii/S0968090X13002593

[25] "Rolling horizon control framework for driver assistance systems. Part II: Cooperative sensing and cooperative control," *Transp. Res. Part C: Emerg. Technol.*, vol. 40, pp. 290–311, 2014. [Online]. Available: https://www.sciencedirect.com/science/article/pii/S0968090X13002611

[26] Y. Zheng, S. E. Li, K. Li, F. Borrelli, and J. K. Hedrick, "Distributed model predictive control for heterogeneous vehicle platoons under unidirectional topologies," *IEEE Trans. Control Syst. Technol.*, vol. 25, no. 3, pp. 899–910, May 2017.

[27] C. Zhai, F. Luo, Y. Liu, and Z. Chen, "Ecological cooperative look-ahead control for automated vehicles travelling on freeways with varying slopes," *IEEE Trans. Veh. Technol.*, vol. 68, no. 2, pp. 1208–1221, Feb. 2019.

[28] M. Lorenzen, M. Cannon, and F. Allgöwer, "Robust MPC with recursive model update," *Automatica*, vol. 103, pp. 461–471, 2019. [Online]. Available: https://www.sciencedirect.com/science/article/pii/S0005109819300731

[29] L. Dai, F. Yang, Z. Qiang, and Y. Xia, "Robust self-triggered MPC with fast convergence for constrained linear systems," *J. Franklin Inst.*, vol. 356, no. 3, pp. 1446–1467, 2019. [Online]. Available: https://www.sciencedirect.com/science/article/pii/S0016003219300018

[30] C. Liu, H. Li, J. Gao, and D. Xu, "Robust self-triggered min-max model predictive control for discrete-time nonlinear systems," *Automatica*, vol. 89, pp. 333–339, 2018. [Online]. Available: https://www.sciencedirect.com/science/article/pii/S0005109817306210

[31] Y.-J. Pan, "Decentralized robust control approach for coordinated maneuvering of vehicles in platoons," *IEEE Trans. Intell. Transp. Syst.*, vol. 10, no. 2, pp. 346–354, Jun. 2009.

[32] Y. Bian, S. E. Li, W. Ren, J. Wang, K. Li, and H. X. Liu, "Cooperation of multiple connected vehicles at unsignalized intersections: Distributed observation, optimization, and control," *IEEE Trans. Ind. Electron.*, vol. 67, no. 12, pp. 10 744–10 754, Dec. 2020.

[33] Y. Wu, S. E. Li, J. Cortés, and K. Poolla, "Distributed sliding mode control for nonlinear heterogeneous platoon systems with positive definite topologies," *IEEE Trans. Control Syst. Technol.*, vol. 28, no. 4, pp. 1272–1283, Jul. 2020.

[34] F. Gao, X. Hu, S. E. Li, K. Li, and Q. Sun, "Distributed adaptive sliding mode control of vehicular platoon with uncertain interaction topology," *IEEE Trans. Ind. Electron.*, vol. 65, no. 8, pp. 6352–6361, Aug. 2018.

[35] S. Wen and G. Guo, "Distributed trajectory optimization and sliding mode control of heterogenous vehicular platoons," *IEEE Trans. Intell. Transp. Syst.*, to be published, doi: 10.1109/TITS.2021.3066688.

[36] G. Guo and D. Li, "Adaptive sliding mode control of vehicular platoons with prescribed tracking performance," *IEEE Trans. Veh. Technol.*, vol. 68, no. 8, pp. 7511–7520, Aug. 2019.

[37] X. Guo, J. Wang, F. Liao, and R. S. H. Teo, "Distributed adaptive integrated-sliding-mode controller synthesis for string stability of vehicle platoons," *IEEE Trans. Intell. Transp. Syst.*, vol. 17, no. 9, pp. 2419–2429, Sep. 2016.

[38] J.-W. Kwon and D. Chwa, "Adaptive bidirectional platoon control using a coupled sliding mode control method," *IEEE Trans. Intell. Transp. Syst.*, vol. 15, no. 5, pp. 2040–2048, Oct. 2014.

[39] Y. Li, C. Tang, S. Peeta, and Y. Wang, "Integral-sliding-mode braking control for a connected vehicle platoon: Theory and application," *IEEE Trans. Ind. Electron.*, vol. 66, no. 6, pp. 4618–4628, Jun. 2019.

[40] J. Wang, X. Luo, L. Wang, Z. Zuo, and X. Guan, "Integral sliding mode control using a disturbance observer for vehicle platoons," *IEEE Trans. Ind. Electron.*, vol. 67, no. 8, pp. 6639–6648, Aug. 2020.

[41] J. Wang, X. Luo, J. Yan, and X. Guan, "Distributed integrated sliding mode control for vehicle platoons based on disturbance observer and multi power reaching law," *IEEE Trans. Intell. Transp. Syst.*, vol. 23, no. 4, pp. 3366–3376, Apr. 2022.

[42] Wen-Hua Chen, D. J. Ballance, P. J. Gawthrop, and J. O'Reilly, "A nonlinear disturbance observer for robotic manipulators," *IEEE Trans. Ind. Electron.*, vol. 47, no. 4, pp. 932–938, Aug. 2000.

[43] Wen-Hua Chen, "Disturbance observer based control for nonlinear systems," *IEEE/ASME Trans. Mechatronics*, vol. 9, no. 4, pp. 706–710, Dec. 2004.

[44] W. Chen, J. Yang, L. Guo, and S. Li, "Disturbance-observer-based control and related methods–An overview," *IEEE Trans. Ind. Electron.*, vol. 63, no. 2, pp. 1083–1095, Feb. 2016.

[45] J. A. Moreno and M. Osorio, "A Lyapunov approach to second-order sliding mode controllers and observers," in *Proc. 47th IEEE Conf. Decis. Control*, 2008, pp. 2856–2861.

[46] A. Levant, "Principles of 2-sliding mode design," *Automatica*, vol. 43, no. 4, pp. 576–586, 2007. [Online]. Available: https://www.sciencedirect.com/science/article/pii/S0005109806004432

[47] J. A. Moreno and M. Osorio, "Strict Lyapunov functions for the super-twisting algorithm," *IEEE Trans. Autom. Control*, vol. 57, no. 4, pp. 1035–1040, Apr. 2012.

[48] L. Fridman and A. Levant, "Higher order sliding modes as a natural phenomenon in control theory," in *Robust Control via Variable Structure and Lyapunov Techniques*, F. Garofalo and L. Glielmo, Eds., Berlin, Heidelberg, Germany: Springer, 1996, pp. 107–133.

[49] A. Chalanga, S. Kamal, L. M. Fridman, B. Bandyopadhyay, and J. A. Moreno, "Implementation of super-twisting control: Super-twisting and higher order sliding-mode observer-based approaches," *IEEE Trans. Ind. Electron.*, vol. 63, no. 6, pp. 3677–3685, Jun. 2016.
[50] K. Yi and Y. D. Kwon, "Vehicle-to-vehicle distance and speed control using an electronic-vacuum booster," *JSAE Rev.*, vol. 22, no. 4, pp. 403–412, 2001. [Online]. Available: https://www.sciencedirect.com/science/article/pii/S0389430401001230
[51] M. Trudgen and J. Mohammadpour, "Robust cooperative adaptive cruise control design for connected vehicles," in *Proc. ASME 2015 Dyn. Syst. Control Conf.*, 2015, pp. 28–30.
[52] A. Levant, "Robust exact differentiation via sliding mode technique," *Automatica*, vol. 34, no. 3, pp. 379–384, 1998. [Online]. Available: https://www.sciencedirect.com/science/article/pii/S0005109897002094

Jianshan Zhou received the B.Sc., the M.Sc., and the Ph.D. degrees in traffic information engineering and control from Beihang University, Beijing, China, in 2013, 2016 and 2020, respectively. From 2017 to 2018, he was a Visiting Research Fellow with the School of Informatics and Engineering, University of Sussex, Brighton, U.K. He is currently a Postdoctoral Research Fellow supported by the Zhuoyue Program of Beihang University and the National Postdoctoral Program for Innovative Talents, and is/was the Technical Program Session Chair with the IEEE EDGE 2020, TPC Member with the IEEE VTC2021-Fall track, and Youth Editorial Board Member of the Unmanned Systems Technology. He is the author or coauthor of more than 20 international scientific publications. His research interests include the modeling and optimization of vehicular communication networks and air-ground cooperative networks, the analysis and control of connected autonomous vehicles, and intelligent transportation systems. He was the recipient of the First Prize in the Science and Technology Award from the China Intelligent Transportation Systems Association in 2017, First Prize in the Innovation and Development Award from the China Association of Productivity Promotion Centers in 2020, National Scholarships in 2017 and 2019, Outstanding Top-Ten Ph.D. Candidate Prize from Beihang University in 2018, Outstanding China-SAE Doctoral Dissertation Award in 2020, and Excellent Doctoral Dissertation Award from Beihang University in 2021.

Daxin Tian (Senior Member, IEEE) received the Ph.D. degree in computer application technology from Jilin University, Changchun, China, in 2007. He is currently a University Professor with the School of Transportation Science and Engineering, Beihang University, Beijing, China. His research interests include intelligent transportation systems, autonomous connected vehicles, swarm intelligence, and mobile computing. He was the recipient of the Changjiang Scholars Program (Young Scholar) of the Ministry of Education of China in 2017, National Science Fund for Distinguished Young Scholars in 2018, and Distinguished Young Investigator of the China Frontiers of Engineering in 2018.

Zhengguo Sheng (Senior Member, IEEE) received the B.Sc. degree from the University of Electronic Science and Technology of China, Chengdu, China, in 2006, and the M.S. and the Ph.D. degrees from Imperial College London, London, U.K., in 2007 and 2011, respectively. He is currently a Senior Lecturer with the University of Sussex, Brighton, U.K. He was with UBC, Vancouver, BC, Canada, as a Research Associate and with Orange Labs, Santa Monica, CA, USA, as a Senior Researcher. He has more than 100 publications. His research interests include IoT, vehicular communications, and cloud/edge computing.

Xuting Duan received the Ph.D. degree in traffic information engineering and control from Beihang University, Beijing, China, in 2017. He is currently an Assistant Professor with the School of Transportation Science and Engineering, Beihang University. His research focuses on vehicular Ad Hoc networks.

Guixian Qu received the B.Sc. degree in transportation engineering from the Shandong University of Technology, Shandong, China, in 2012, the M.Sc. and the Ph.D. degrees from the Beijing University of Technology, Beijing, China, in 2014 and 2019, respectively. She was a Postdoctoral Research Fellow with Beihang University. She is currently an Research Fellow of Research Institute of Aero-Engine, Beihang University, Beijing, China. Her research interests include intelligent transportation systems, dynamics modeling and control, and collaborative design of aero-engine systems.

Dongpu Cao (Member, IEEE) received the Ph.D. degree from Concordia University, Montreal, QC, Canada, in 2008. He is the Canada Research Chair of Driver Cognition and Automated Driving, and currently an Associate Professor and the Director of Waterloo Cognitive Autonomous Driving (CogDrive) Laboratory, University of Waterloo, Waterloo, ON, Canada. He has contributed more than 200 papers and three books. His research include driver cognition, automated driving, and cognitive autonomous driving. He was the recipient of the SAE Arch T. Colwell Merit Award in 2012, IEEE VTS 2020 Best Vehicular Electronics Paper Award and three Best Paper Awards from the ASME and IEEE conferences.

Prof. Cao is the Deputy Editor-in-Chief of *IET Intelligent Transport Systems Journal*, and an Associate Editor for IEEE TRANSACTIONS ON VEHICULAR TECHNOLOGY, IEEE TRANSACTIONS ON INTELLIGENT TRANSPORTATION SYSTEMS, IEEE/ASME TRANSACTIONS ON MECHATRONICS, IEEE TRANSACTIONS ON INDUSTRIAL ELECTRONICS, IEEE/CAA JOURNAL OF AUTOMATICA SINICA, IEEE TRANSACTIONS ON COMPUTATIONAL SOCIAL SYSTEMS, and *ASME Journal of Dynamic Systems, Measurement and Control*. He was the Guest Editor of Vehicle System Dynamics, IEEE TRANSACTIONS ON SMC: SYSTEMS and IEEE INTERNET OF THINGS JOURNAL. He is on the SAE Vehicle Dynamics Standards Committee and acts as the Co-Chair of IEEE ITSS Technical Committee on Cooperative Driving. Prof. Cao is an IEEE VTS Distinguished Lecturer.

Xuemin Shen (Fellow, IEEE) received the Ph.D. degree in electrical engineering from Rutgers University, New Brunswick, NJ, USA, in 1990. He is currently a University Professor with the Department of Electrical and Computer Engineering, University of Waterloo, Canada. His research interests include network resource management, wireless network security, Internet of Things, 5G and beyond, and vehicular Ad Hoc and sensor networks. Dr. Shen is a registered Professional Engineer of Ontario, Canada, an Engineering Institute of Canada Fellow, a Canadian Academy of Engineering Fellow, Royal Society of Canada Fellow, Chinese Academy of Engineering Foreign Member, and Distinguished Lecturer of the IEEE Vehicular Technology Society and Communications Society.

Dr. Shen was the recipient of the R.A. Fessenden Award in 2019 from IEEE, Canada, Award of Merit from the Federation of Chinese Canadian Professionals (Ontario) in 2019, James Evans Avant Garde Award in 2018 from the IEEE Vehicular Technology Society, Joseph LoCicero Award in 2015 and Education Award in 2017 from the IEEE Communications Society, and Technical Recognition Award from Wireless Communications Technical Committee (2019) and AHSN Technical Committee (2013). He was also the recipient of the Excellent Graduate Supervision Award in 2006 from the University of Waterloo and the Premier's Research Excellence Award in 2003 from the Province of Ontario, Canada. He was the Technical Program Committee Chair/Co-Chair of IEEE Globecom'16, IEEE Infocom'14, IEEE VTC'10 Fall, IEEE Globecom'07, and the Chair of the IEEE Communications Society Technical Committee on Wireless Communications. Dr. Shen is the elected IEEE Communications Society Vice President for Technical & Educational Activities, Vice President for Publications, Member-at-Large on the Board of Governors, Chair of the Distinguished Lecturer Selection Committee, Member of IEEE ComSoc Fellow Selection Committee. He was/is the Editor-in-Chief of the IEEE IoT JOURNAL, *IEEE Network*, *IET Communications,* and *Peer-to-Peer Networking and Applications*.